From THE DEPARTMENT OF CLINICAL NEUROSCIENCE
Karolinska Institutet, Stockholm, Sweden

DUAL-ENERGY IMAGING IN STROKE:

FEASIBILITY OF DUAL-LAYER DETECTOR CONE-BEAM COMPUTED TOMOGRAPHY

Fredrik Ståhl

Karolinska Institutet

Stockholm 2023

All previously published papers were reproduced with permission from the publisher.
Published by Karolinska Institutet.
Printed by Universitetsservice US-AB, 2023

ISBN 978-91-8017-147-2
Cover illustration: A collage of images generated through DALL-E, creating a shape with slight resemblance to a dual-layer detector, as seen from one side.

Dual-energy imaging in stroke: Feasibility of dual-layer detector cone-beam computed tomography

Thesis for Doctoral Degree (Ph.D.)

By

Fredrik Ståhl

The thesis will be defended in public at A6:04 Lars Leksell, Karolinska University Hospital in Solna, Friday 20 October 2023 at 09:15.

Principal Supervisor:
Associate Professor Anna Falk Delgado
Karolinska Institutet
Department of Clinical Neuroscience
Division of Neuro

Co-supervisor(s):
Doctor Gavin Poludniowski
Karolinska Institutet
Department of Clinical Science, Intervention and Technology (CLINTEC)
Division of Functional Imaging and Technology

Professor Staffan Holmin
Karolinska Institutet
Department of Clinical Neuroscience
Division of Neuro

Opponent:
Associate Professor Johan Wassélius
Lund University
Department of Diagnostic Radiology
Division of Neuroradiology

Examination Board:
Associate Professor Elias Johansson
University of Gothenburg
Institute of Neuroscience and Physiology
Department of Clinical Neuroscience

Associate Professor Mischa Woisetschläger
Linköping University
Department of Health, Medicine and Caring Sciences
Division of Diagnostics and Specialist Medicine

Professor Magnus Båth
University of Gothenburg
Institute of Clinical Sciences
Department of Medical Radiation Sciences

Panta rhei

– Heraclitus

Popular science summary of the thesis

If stroke is suspected, the patient needs to be diagnosed through imaging, typically computed tomography (CT), in order to make an adequate treatment decision. Often, symptoms are caused by a clotted artery, resulting in a lack of oxygen delivery to the brain. In cases where the clot is causing significant symptoms and blood thinning treatment is not expected to work, the patient needs to be transported to a unit that can treat the clot effectively by mechanically pulling it out. This is done with minimally invasive instruments under X-ray guidance in a specialized interventional unit where flat X-ray detectors are used. Transferring the patient from the diagnostic CT to an interventional unit consumes time and resources. The extent of brain damage is dependent on time to successful clot removal.

A flat X-ray detector can be rotated around the patient to acquire images similar to CT (cone-beam CT). However, the technique is typically insufficient for a reliable diagnosis due to poor distinction between different tissues and prominent image artifacts. Through an innovative solution, the flat detector could be modified so that it separates X-rays with different energies, thereby improving the diagnostic quality. Consequently, stroke patients could potentially be diagnosed and treated in the same room. The goal of this thesis was to study the diagnostic utility of the X-ray energy separation technique, first in CT where it is already used to some extent and then in cone-beam CT using a novel flat X-ray detector.

The first paper indicated that CT images utilizing X-ray energy separation impact the assessment of hypoxic brain regions in acute stroke patients. Images representing a particular virtual energy had the best diagnostic value. The second paper characterized a prototype cone-beam CT system with the modified flat X-ray detector through image experiments on different materials. The images showed that the detector had potential utility in diagnostic imaging. The third and fourth paper studied the modified detector in a group of stroke patients. These papers indicated that images representing certain virtual energies were not inferior to the corresponding conventional CT images without contrast medium (paper III) or with contrast medium in the arteries of the brain (paper IV), under certain conditions. In summary, this thesis shows that stroke diagnosis directly in the interventional unit is possible using the modified detector, but also that there are opportunities for further development.

Populärvetenskaplig sammanfattning

Patienter med misstänkt stroke behöver vid ankomst till sjukhus undersökas med bildgivande diagnostik, i regel datortomografi (DT), inför beslut om rätt behandling. Ofta beror symptomen på en propp i hjärnans kärl som orsakar syrebrist. I de fall proppen orsakar påtagliga symptom och blodförtunnande behandling inte förväntas fungera behöver patienten flyttas till en enhet som kan behandla proppen effektivt genom att mekaniskt dra eller suga ut den. Detta görs med minimalinvasiv teknik under röntgenvägledning på en särskild interventionell enhet där man använder sig av platta röntgendetektorer. Att förflytta patienter från bildgivande DT till en interventionsenhet förbrukar tid och resurser. En effektiv vårdkedja är avgörande för patientens prognos.

Med en platt röntgendetektor kan man genom en roterande rörelse runt patienten ta bilder (volymtomografi) som efter databehandling går att bedöma på liknande sätt som vid DT. Distinktionen mellan olika vävnader och därmed den diagnostiska säkerheten är dock idag bristfällig. Den platta detektorn skulle genom en innovativ lösning kunna modifieras så att den separerar röntgenstrålar med olika energi, och därmed förbättra den diagnostiska bilden. På så sätt skulle strokepatienter potentiellt kunna diagnosticeras och behandlas i samma rum. Målet med avhandlingen var att utvärdera denna energiseparerande teknik, först med DT där tekniken redan används i vissa sammanhang och sedan genom volymtomografi utförd med en ny modifierad platt röntgendetektor.

Det första arbetet visade att DT-bilder som tagits med energiseparerande teknik påverkar bedömningen av områden med syrebrist i hjärnan hos strokepatienter. Bilder representerande en särskild virtuellt framställd energi hade bäst diagnostiskt värde. Det andra arbetet karaktäriserade genom experimentella test volymtomografiska bilder utförda med den modifierade platta röntgendetektorn. Testerna visade att detektorn var användbar med potentiell nytta för diagnostisk bildtagning. Det tredje och fjärde arbetet studerade bilder tagna med den modifierade detektorn på strokepatienter. Arbetena visade att bilderna representerande särskilda virtuella energier inte var sämre än motsvarande DT-bilder utan kontrastmedel (arbete III) eller med kontrastmedel i hjärnans kärl (arbete IV), under vissa förutsättningar. Sammantaget visar avhandlingens arbeten att bilddiagnostik av strokepatienter direkt på interventionsenhet är möjlig med den modifierade detektorn, men att utvecklingsmöjligheter finns.

Abstract

Background: Dual-energy computed tomography (DECT) is increasingly available and used in the standard diagnostic setting of ischemic stroke patients. For stroke patients with suspected large vessel occlusion, cone-beam computed tomography (CBCT) in the interventional suite could be an alternative to CT to shorten door to thrombectomy time. This approach could potentially lead to an improved patient outcome. However, image quality in CBCT is typically limited by artifacts and poor differentiation between gray and white matter. A dual-layer detector CBCT (DL-CBCT) system could be used to separate photon energy spectra with the potential to increase visibility of clinically relevant features, and acquire additional information.

Purpose: Paper I evaluated how a range of DECT virtual monoenergetic images (VMI) impact identification of early ischemic changes, compared to conventional polyenergetic CT images. **Paper II** characterized the performance of a novel DL-CBCT system with regards to clinically relevant imaging features. **Paper III & IV** investigated if DL-CBCT VMIs are sufficient for stroke diagnosis in the interventional suite, compared to reference standard CT.

Methods: Paper I was a retrospective single-center study including consecutive patients presenting with acute ischemic stroke caused by an occlusion of the intracranial internal carotid artery or proximal middle cerebral artery. Automated Alberta Stroke Program Early Computed Tomography Score (ASPECTS) results from conventional images and 40-120 keV VMI were generated and compared to reference standard CT ASPECTS. In **paper II**, a prototype dual-layer detector was fitted into a commercial interventional C-arm CBCT system to enable dual-energy acquisitions. Metrics for spatial resolution, noise and uniformity were gathered. Clinically relevant tissue and iodine substitutes were characterized in terms of effective atomic numbers and electron densities. Iodine quantification was performed and virtual non-contrast (VNC) images were evaluated. VMIs were reconstructed and used for CT number estimation and evaluation of contrast-to-noise ratios (CNR) in relevant tissue pairings. In **paper III and IV**, a

prospective single-center study enrolled consecutive participants with ischemic or hemorrhagic stroke on CT. In **paper III**, hemorrhage detection accuracy, ASPECTS accuracy, subjective and objective image quality were evaluated on non-contrast DL-CBCT 75 keV VMI and compared to reference standard CT. In **paper IV,** intracranial arterial segment vessel visibility and artifacts were evaluated on intravenous DL-CBCT angiography (DL-CBCTA) 70 keV VMI and compared to CT angiography (CTA). In both **paper III and IV**, non-inferiority was determined by the exact binomial test with a one-sided lower performance boundary set to 80% (98.75% CI).

Main results: In **paper I**, 24 patients were included. 70 keV VMI had the highest region-based ASPECTS accuracy (0.90), sensitivity (0.82) and negative predictive value (0.94), whereas 40 keV VMI had the lowest accuracy (0.77), sensitivity (0.34) and negative predictive value (0.80). In **paper II**, the prototype and commercial CBCT had a similar spatial resolution and noise using the same standard reconstruction. For all tissue substitutes, the mean accuracy in effective atomic number was 98.2% (SD 1.2%) and 100.3% (SD 0.9%) for electron density. Iodine quantification had a mean difference of -0.1 (SD 0.5) mg/ml compared to the true concentrations. For VNC images, iodine substitutes with blood averaged 43.2 HU, blood only 44.8 HU, iodine substitutes with water 2.6 HU. A noise-suppressed dataset showed a CNR peak at 40 keV VMI and low at 120 keV VMI. In the same dataset without noise suppression, peak CNR was seen at 70 keV VMI and a low at 120 keV VMI. CT numbers of various clinically relevant objects generally matched the calculated CT number in a wide range of VMIs. In **paper III**, 27 participants were included. One reader missed a small bleeding, however all hemorrhages were detected in the majority analysis (100% accuracy, CI lower boundary 86%, p=0.002). ASPECTS majority analysis had 90% accuracy (CI lower boundary 85%, p<0.001), sensitivity was 66% (individual readers 67%, 69% and 76%), specificity was 97% (97%, 96% and 89%). Subjective and objective image quality metrics were inferior to CT. In **paper IV**, 21 participants had matched image sets. After excluding examinations with scan issues, all

readers considered DL-CBCTA non-inferior to CTA (CI boundary 93%, 84%, 80%, respectively), when assessing arteries relevant in candidates for intracranial thrombectomy. Artifacts were more prevalent compared to CTA.

Conclusions: In **paper I**, automated 70 keV VMI ASPECTS had the highest diagnostic accuracy, sensitivity and negative predictive value overall. Different VMI energy levels impact the identification of early ischemic changes on DECT. In **paper II**, the DL-CBCT prototype system showed comparable technical metrics to a commercial CBCT system, while offering dual-energy capability. The dual-energy images indicated a consistent ability to separate and characterize clinically relevant tissues, blood and iodine. Thus, the DL-CBCT system could find utility in the diagnostic setting. In **paper III**, non-contrast DL-CBCT 75 keV VMI showed non-inferior hemorrhage detection and ASPECTS accuracy to CT. However, image quality was inferior compared to CT, and visualization of small subarachnoid hemorrhages after treatment remains a challenge. In the same stroke cohort, **paper IV** showed non-inferior vessel visibility for DL-CBCTA 70 keV VMI compared to CTA under certain conditions. Specifically, the prototype system had a long scan time and was not capable of bolus tracking which resulted in scan issues. After excluding participants with such issues, DL-CBCTA 70 keV VMI were found non-inferior to CTA.

In summary, the findings of this thesis indicate that DL-CBCT may be sufficient for stroke assessment in the interventional suite with the potential to bypass CT in patients eligible for thrombectomy. However, issues related to the prototype system and the visualization of small hemorrhages highlight the need of further development.

List of scientific papers

I. **Performance of dual layer dual energy CT virtual monoenergetic images to identify early ischemic changes in patients with anterior circulation large vessel occlusion**

Ståhl F, Gontu V, Almqvist H, Mazya MV, Falk Delgado A.
Journal of Neuroradiology. 2021 Mar;48(2):75-81

II. **Performance characterization of a prototype dual-layer cone-beam computed tomography system**

Ståhl F, Schäfer D, Omar A, Van De Haar P, Van Nijnatten F, Withagen P, Thran A, Hummel E, Menser B, Holmberg Å, Söderman M, Falk Delgado A, Poludniowski G.
Medical Physics. 2021;48(11):6740-6754

III. **Stroke evaluation in the interventional suite using dual-layer detector cone-beam CT: a first-in-human prospective cohort study (the Next Generation X-ray Imaging System Trial)**

Ståhl F, Almqvist H, Aspelin Å, Kolloch J, Ghalamkari O, Gontu V, Schäfer D, Van De Haar P, Engel K-J, Van Nijnatten F, Holmberg Å, Mazya MV, Söderman M, Falk Delgado A.
Submitted manuscript

IV. **Dual-Layer Detector Cone-Beam CT Angiography for Stroke Assessment: First-in-Human Results (the Next Generation X-ray Imaging System Trial)**

Ståhl F, Almqvist H, Kolloch J, Aspelin Å, Gontu V, Hummel E, Van Vlimmeren M, Simon M, Thran A, Holmberg Å, Mazya MV, Söderman M, Falk Delgado A.
American Journal Of Neuroradiology. 2023; 44(5): 523-529

Contents

List of abbreviations

aGFR	Absolute Glomerular Filtration Rate
AIS	Acute Ischemic Stroke
ASPECTS	Alberta Stroke Program Early Computed Tomography Score
CBCT	Cone-Beam Computed Tomography
CBCTA	Cone-Beam Computed Tomography Angiography
CI	Confidence Interval
CNR	Contrast-to-Noise Ratio
CS	Compton Scatter
CT	Computed Tomography
CTA	Computed Tomography Angiography
CTP	Computed Tomography Perfusion
DE	Dual-Energy
DECT	Dual-Energy CT
DL	Dual-Layer
ED	Electron Density
EID	Energy Integrating Detector
HU	Hounsfield Units
ICA	Internal Carotid Artery
IQR	Interquartile Range
keV	Kilo-electron volt
kVp	Kilovoltage peak
LVO	Large Vessel Occlusion
MCA	Middle Cerebral Artery
mCTA	Multiphase Computed Tomography Angiography
MRI	Magnetic Resonance Imaging
MTF	Modulation Transfer Function
NEXIS	Next Generation X-ray Imaging System

PCD	Photon Counting Detector
PCCT	Photon Counting Computed Tomography
PE	Photoelectric Effect
rCBF	Relative Cerebral Blood Flow
refASPECTS	Reference standard ASPECTS
SD	Standard Deviation
SNR	Signal-to-Noise Ratio
tPA	Tissue Plasminogen Activator
VMI	Virtual Monoenergetic Images
VNC	Virtual Non Contrast
WL	Window Level
WW	Window Width
Z_{eff}	Effective Atomic Number

Introduction

At the inception of my residency at Karolinska University Hospital, I was approached with the possibility to be involved in the "Next generation X-ray imaging system" (NEXIS) project, a part of the EU-funded Horizon 2020-programme. The project involved a multidisciplinary consortium across Europe that aimed to develop and evaluate a dual-layer flat X-ray detector with the possibility of improved image quality in cone-beam computed tomography (CBCT). After some time, I was given the opportunity to serve as the work package leader for the clinical evaluation of the project.

The clinical use case was to shorten time to treatment for stroke patients with a large vessel occlusion. Typically, patients with symptoms suggestive of stroke are imaged and diagnosed by conventional computed tomography (CT). In the case of a large vessel occlusion, they are then transported to an interventional angiography suite to receive thrombectomy treatment. The interventional suite is equipped with a flat detector capable of CBCT acquisitions, however the image quality is typically considered insufficient for primary diagnostic work-up. Given an improvement in image quality with the novel detector design, a patient with symptoms suggestive of a large vessel occlusion stroke could potentially bypass the CT, and thus receive both diagnosis and treatment in the interventional suite instead.

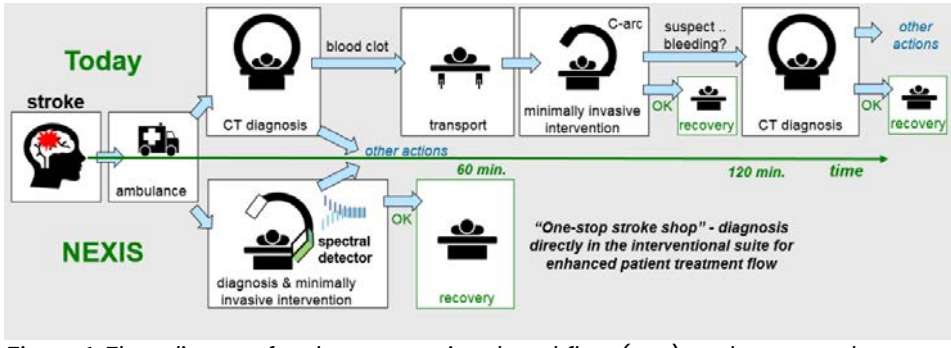

Figure 1. Flow diagram for the conventional workflow (top), and proposed workflow using the NEXIS detector (bottom). Reprinted with permission from Heidrun Steinhauser, project leader of the NEXIS consortium.

1 Literature review

1.1 Stroke burden and associated costs

The World Health Organization estimates that stroke is the second most common cause of death and the third leading cause of disability in the world (1). In 2010 it was concluded that the global burden of stroke is considerable and increasing, with an estimation of 100 million disability-adjusted-life-years lost annually (2). Stroke caused an estimated 6.2 million deaths in 2019 of which the majority occurred in middle- to high income countries (3, 4). Cerebrovascular disease is the most common cause of neurological disability in older adults (5) and contributes substantially to other late complications such as dementia and epilepsy. Stroke incidence rates are increasing rapidly in low-income and middle-income countries (6, 7). In high-income countries, substantial increases in the absolute numbers of individuals affected by stroke are projected due to increasing population life-expectancy, even if stroke incidence rates are reduced or maintained at current levels (6). Globally, the prevalence of stroke was 104.2 million people in 2017, of which 82.4 million accounted for ischemic stroke (4). The prevalence of ischemic stroke increased by 16.1% from 2007 to 2017 (4).

Stroke is also a substantial contributor to healthcare costs. A publication based on data from 2014—2015 estimated the aggregated societal costs for stroke of £26 billion per year in the UK (8). The American Heart Association estimated that the yearly direct and indirect costs of stroke were $56.5 billion in 2018—2019 (9). These costs are expected to increase to $94.3 billion in 2035 (4).

1.2 Ischemic stroke

87% of all stroke is due to ischemia (9). Ischemic stroke is caused by acute occlusion of an artery leading to immediate reduction in blood flow within the corresponding cerebrovascular territory. The size and site of the occlusion, and the efficiency of compensatory collateral blood flow, determines the extent of

impaired blood flow and resulting neurological symptoms from insufficiently perfused brain tissue, either infarcted or at risk of infarction (ischemic penumbra). Early spontaneous recanalization may occur from endogenous release of tissue plasminogen activator (tPA), however for many patients, and particularly in those with large occlusions, the endogenous release of tPA is not sufficient to prevent infarcted cerebral tissue caused by vessel occlusion (10, 11).

1.3 Stroke treatment

Acute ischemic stroke (AIS) can be treated either by administering a thrombolytic drug (thrombolysis), or by thrombectomy where the blocking thrombus is retrieved from the occluded vessel with an endovascular device. Both treatment strategies can be used together in the case of a large vessel occlusion (LVO) (12). In Sweden 2021, 17% of all patients suffering from acute ischemic stroke were treated with a reperfusion treatment: 13% received thrombolysis, 6% thrombectomy (3% received both) (12).

1.3.1 Thrombolysis

Clot-dissolving (thrombolytic) drugs, typically intravenous recombinant tissue plasminogen activators, can significantly improve the prognosis for a patient with AIS if administered within 4.5 hrs after symptom onset (13, 14). A meta-analysis suggested that functional outcome can be improved if thrombolysis is administered within 9 hours in selected cases guided by perfusion imaging (15). Until 2015, thrombolysis was the only treatment for AIS with robust scientific evidence. Although important, it has been shown that thrombolysis has a very small likelihood of successful recanalization when the thrombus measures 8 mm or more (10). Large thrombi commonly occlude the proximal intracranial arteries, termed LVO. The proximal location of a LVO typically leads to substantial neurological deficits and a poor prognosis without successful treatment (16).

1.3.2 Endovascular treatment

A blood clot/thrombus in a proximal intracranial artery can be removed by an endovascular procedure termed thrombectomy. The thrombectomy aims to achieve arterial recanalization and thus restoration of blood flow and oxygen delivery to brain tissue. Typically, the femoral artery is punctured with a needle and the intracranial arterial vasculature is subsequently accessed using a catheter system under X-ray guidance. Endovascular treatment in combination with intravenous thrombolysis for patients with AIS and LVO using second-generation devices have shown to improve functional outcome in several large randomized clinical trials (17-21). These studies provided compelling evidence for the beneficial results of thrombectomy in patients with LVO of the anterior circulation presenting within 6 to 12 hours of symptom onset and has since 2015 been established practice worldwide.

Furthermore, the DAWN and DEFUSE 3 trials published in 2018 provided insights that thrombectomy can be a beneficial treatment option up to 24 hours after symptom onset, thus making endovascular recanalization a possible treatment option for an even larger patient group (22, 23). These studies both used "mismatch" imaging concepts separating irreversible ischemic tissue from potentially salvageable tissue to select patients for thrombectomy.

1.4 X-ray imaging in stroke

Multiple imaging protocols are used together to diagnose patients presenting with symptoms consistent with acute stroke. A reliable diagnosis is essential to determine the most beneficial treatment strategy for the patient. Studies that established the efficacy of modern endovascular recanalization in anterior circulation large vessel occlusion (LVO) predominantly used non-contrast computed tomography (CT) combined with vascular (17-21) and perfusion imaging (19, 20) for patient selection. In the following chapters, technical,

diagnostic and clinical aspects of CT imaging will be covered with a focus on stroke.

1.4.1 Fundamentals of Computed Tomography

Sir Godfrey N. Hounsfield and Allan MacLeod Cormack shared the Nobel Prize for Physiology and Medicine in 1979. In his groundbreaking paper on CT in 1973, Sir Hounsfield described a system in which X-ray transmission readings were taken at a multitude of angles through a cranium, calculated on a computer and shown as a series of axial pictures ("slices") through the head (24). The modern technique typically involves a fan-shaped X-ray beam emitted from a X-ray tube rotating around the patient. The X-rays (photons) emitted from the tube are captured on the opposite side of the patient by a number of detector elements. The technique has evolved from single slice axial acquisitions to multi-slice spiral acquisitions, utilizing multiple detector rows and simultaneous movement of the patient table (25). These innovations enable a quick image acquisition and volume (multiplanar, 3D) image reconstructions which are typical features of modern CT imaging (25). Today, CT scanners are a mainstay in modern medical diagnostics, with an estimated 14 153 scanners in the Unites States alone in 2021 (26).

Photons (X-rays) interact with matter in different ways depending on the energy of the incident photons as well as the atomic number and the density of the material or tissue. These factors determine the linear attenuation coefficient of a material, which translates to the CT number, also called Hounsfield Units (HU), which is a measure of radiodensity. Today, the HU is the common quantitative measurement displayed in a grayscale of pixels used by radiologists in the interpretation of CT images. The HU is a relative scale, calculated through a linear transformation of the linear attenuation coefficient of the photon beam, where water and air at standard pressure and temperature are defined to 0 and -1000 HU, respectively (24, 27). Although often used for quantitative measurements, HU is known to be dependent on various CT parameters, including the design of the

individual system, reconstruction algorithm, X-ray kilovoltage, position of the object, scatter effects and various other artifacts such as beam hardening (28). Even though modern CT systems can correct for some of these factors in the image reconstruction process, HU consistency is typically checked and calibrated at regular intervals (25).

1.4.2 Non-contrast CT

Non-contrast CT is a widely available diagnostic tool used to investigate the presence of various intracranial pathologies, including cerebral ischemia (29). A non-contrast CT scan is typically the first diagnostic investigation to be done in order to exclude the presence of intracranial hemorrhage (i.e. hemorrhagic stroke) and extensive infarction, as both are contraindications for intravenous thrombolytic therapy. Today, non-contrast CT provides sub-millimeter resolution in x, y as well as z direction (3D) and is an efficacious diagnostic imaging technique because of high resolution, high availability and quick scan time.

1.4.2.1 Alberta stroke program early CT score

The Alberta stroke program early CT score (ASPECTS) is a well-established ordinal 10-point scoring system typically applied to non-contrast CT to assess the extent and localization of ischemic damage to cerebral regions supplied by the middle cerebral artery (30). ASPECTS has been shown to correlate with functional outcome and death (31), with a high score indicating that fewer cerebral regions are ischemic, compared to a low score. It has been used to assess patient eligibility for large clinical trials and is today an important tool in clinical routine for ascertaining eligibility of patients with suspected acute anterior LVO for endovascular thrombectomy (18, 19, 21, 22). More recently, an automated ASPECTS algorithm (e-ASPECTS) has been shown to perform non-inferior to neuroradiologists (32) and has greater sensitivity than junior stroke

physicians (33) in scoring ASPECTS on CT scans of patients with acute anterior circulation LVO. Moreover, e-ASPECTS correlates with functional outcome after mechanical thrombectomy (34, 35).

1.4.3 CT angiography

CT angiography (CTA) serves the purpose of mapping the cerebral vascular anatomy as well as identifying any occlusion, stenosis or vessel anomaly which could have implications on treatment strategy. CTA is performed with, and synchronized to, intravenous iodine contrast agent administration. With CTA, one can identify the thrombus in the case of an ischemic stroke. Approximately 80% of all ischemic strokes occur in the anterior circulation. Currently, there is substantial evidence (16-22, 36) that it is possible to access and extract occlusions located in proximal anterior circulation vessels such as the internal carotid artery (ICA) and middle cerebral artery (MCA) M1 and proximal M2 segments; an occlusion in these vessel territories constitutes the core definition of a LVO (37). In addition, the LVO definition encompasses occlusions of the distal vertebral artery and basilar artery and are therefore also deemed accessible by thrombectomy (37).

1.4.4 CT perfusion

Using dynamic information provided by CT perfusion (CTP), early manifest infarctions not visible on non-contrast CT can be detected. This information is crucial as manifest ischemia increases the risk and decreases potential benefit of endovascular recanalization therapies. Equally important, dynamic imaging also visualizes tissue with decreased blood flow at risk of manifest ischemia (penumbra) that could potentially be salvaged by endovascular recanalization.

Similar to CTA, CTP is performed with and synchronized to intravenous iodine contrast agent administration. However, CTP involves repeated scans over the head (usually 17—35 sweeps) over the course of 40—60 seconds. The

assessment of CTP involves a "mismatch" concept where the estimated ischemic core is subtracted from the total critical perfusion deficit. Several parameters and thresholds have been described, most frequently validated by comparing the final infarct volume on magnetic resonance imaging in cases where either no reperfusion or complete reperfusion were achieved (38). A relative cerebral blood flow (rCBF) below 30% of the normally perfused brain tissue has been validated as a robust definition of ischemic core (38). Typically, the critical perfusion deficit is defined by parameters related to the temporal dynamics of the blood concentration. A delay over six seconds for the parameter Tmax has shown to be a good estimate of critical hypoperfusion destined to infarction in the absence of reperfusion (38). Multiple software tools are available to assess CTP parameters, with some agreement differences (38, 39). Importantly, it has been shown that the ischemic core may be overestimated in patients with LVO imaged soon after symptom onset when using the rCBF 30% definition (38, 40). This emphasizes caution when evaluating CTP image data, which should be interpreted as a hemodynamic state rather than true tissue fate, as other factors needs to be taken into consideration (40).

The HERMES collaboration (16) indicated that dynamic imaging was beneficial in selecting patients for thrombectomy, and subsequent large studies such as DAWN and DEFUSE 3 (22, 23) both used dynamic imaging for patient selection in an extended time window (up to 24 hrs. from symptom onset). Similarly, patient selection by perfusion imaging for thrombolysis in an extended time frame (4.5—9.0 hrs.) has also been proven to correlate with beneficial outcome (15, 41). Accordingly, CTP has rapidly become an established practice at many comprehensive stroke centers worldwide when assessing patients with suspected AIS.

1.4.5 Multiphase CT angiography

An alternative or complement to CTP to assess vessel perfusion dynamics is to use multiphase CTA (mCTA). This technique usually involves three consecutive

CTA scans, approximately 8 seconds apart. mCTA has been shown to correlate with functional outcome in patients better than a single-phase CTA (42) and determined a reliable tool for imaging selection in patients with AIS (43). Moreover, mCTA has been shown to predict tissue fate similar to CTP in patients with AIS (44). The assessment of mCTA does not necessarily involve additional software tool analysis (which is required for CTP), and thus makes mCTA easier to use and less dependent on advanced processing algorithms.

1.4.6 Cone-beam CT

Flat detectors are used in a multitude of clinical imaging applications. In interventional neuroradiology, endovascular recanalization is performed with X-ray guidance in an interventional suite equipped with a flat detector C-arm system (45). The flat detector is predominantly used for 2D image guidance, however, it can also be used for diagnostic 3D imaging by rotating the X-ray tube and opposed detector around the patient and reconstructing the resulting 3D volume. This imaging modality is termed cone-beam CT (CBCT). CBCT using indirect-detection flat detectors for bone and soft-tissue assessment was introduced in 2000 (46). The technique has similarities to conventional CT, but acquires an entire volumetric image through a single rotation by utilizing a cone-shaped X-ray beam and a large flat image detector (46). Due to space constraints in interventional procedures, an incomplete rotation of the detector (such as 200 degrees) can be employed, resulting in the need to weight the input data for the reconstruction (47).

CBCT is frequently used in conjunction with interventional procedures to assess anatomy and associated pathology. It can be used to depict iodine contrast enhanced blood vessels, visualize target lesions, for periprocedural information such as stent placement, as well as for detection of procedure related complications such as hemorrhage (48-51). The technique is also used to assess bone morphology of the middle and inner ear, and in dentistry applications (52-54).

One specific challenge associated with CBCT is increased X-ray scatter due to the cone angle and comparatively large detector (55). Similar to CT, CBCT also suffers from appreciable beam-hardening effects (56). Scatter, beam-hardening and other effects contribute to artifact formation (such as cupping and streak artifacts), increased noise, decreased contrast and affects the quantitative measure of radiodensity in CBCT (55-57). Consequently, CBCT images typically have a quantitative gray scale not identical, but with strong correlation to HU, and can be referred to simply as a "CT number" (46, 58).

1.4.6.1 Clinical limitations and emerging possibilities of CBCT

For LVO stroke patients, CBCT with an interventional C-arm system could be an alternative to CT to shorten the door to thrombectomy time (59, 60). However, CBCT is less sensitive than CT in identifying hemorrhage (48, 61) and early ischemic changes (62-64). Due to several factors, including X-ray scatter, detector limitations and beam hardening artifacts, flat detector systems typically provide limited discernment of low contrast tissues, such as gray and white matter in the brain (51, 65). Furthermore, conventional CBCT is limited to integrated full energy spectrum (polyenergetic) image acquisitions and cannot be used for material or energy selective imaging or to estimate tissue properties such as effective atomic number (Z_{eff}) or electron density (ED).

Some studies indicate that latest generation CBCT could replace CT in the setting of acute stroke, with reference to ASPECTS score accuracy, hemorrhage detection and image quality (65-67). Studies on intravenous CBCT angiography (CBCTA) have shown equal or better results compared to CTA for the diagnosis of proximal middle cerebral artery occlusions or intracranial stenoses (62, 63). A study in 10 patients indicated superior image quality results in multiple CBCTA arterial segments compared to CTA, however the patient cohort was biased, heterogenous and only individual vessel segments were analyzed (68). A retrospective study on 16 stroke patients with LVO of the anterior circulation showed that CBCTA generated from a volume perfusion scan could reliably

identify the occlusion site of the internal carotid and the proximal middle cerebral artery, however the study did not find CBCTA superior to CTA (69).

Three single-center studies (two observational and one randomized clinical trial) have indicated that transferring patients with stroke symptoms directly to the interventional suite may reduce intra-hospital time delays and improve functional outcome in those subjected to thrombectomy (60, 70, 71). A multicenter trial is being conducted to study the generalizability of the results (72).

Figure 2. An interventional bi-plane system with flat detectors capable of performing 2D X-ray acquisitions as well as 3D CBCT acquisitions. The CBCT acquisitions are performed using the floor-mounted X-ray tube and detector. Reprinted with permission from Heidrun Steinhauser, project leader of the NEXIS consortium.

1.5 Dual-energy imaging

In 1953, B. Jacobson presented "dichromography", a method to measure the concentration of iodine in X-ray images using two different energy exposures, which may be regarded as the first medical application of dual-energy imaging

(73). Today, "dual-energy" is a common terminology used in X-ray imaging where information from two different X-ray spectra are used to generate an image (74).

The main photon interactions in the energy range used for diagnostic imaging are through Compton Scattering (CS) and Photoelectric Effect (PE). Essentially, the composition of the tissue or material (density and atomic number) determines the probability of a photon of a certain energy to interact by either CS or PE. The PE interaction component shows a greater energy dependency in the diagnostic energy range compared to the CS component, which is fundamental in the generation of dual-energy information (74).

1.5.1 Dual-energy CT

Dual energy CT (DECT) was first proposed in 1976 (75) and subsequently implemented in a commercial CT system in the 1980s (76). Dual-energy imaging have gained attention over the last decades, with an associated increase in clinical DECT applications to improve image quality and to extract additional image information (74, 77, 78).

Detectors in conventional and dual-energy CT typically consists of a scintillator material where the incident photon energy is converted to a light signal (indirect detection). These detectors are termed energy integrating detectors (EIDs), where the detected signal is proportional to the total energy deposited from all photons incident on the detector at a given time, with no information about individual photon energy (25, 79). To enable dual-energy information in one single CT acquisition, different solutions have been employed, including dual-source imaging, dual-layer detectors, fast kilovoltage peak (kVp) switching and split filter techniques (80-83).

1.5.1.1 Imaging applications with a focus on stroke

Material decomposition is typically used to extract dual-energy information. This is accomplished by dividing the acquired projection or image data into basis function pairs based on the photon energy and linear attenuation coefficients (74, 84). By combining the two basis functions, it is possible to derive energy selective images, such as virtual monoenergetic images (VMI) or material specific images such as iodine maps, virtual non-contrast (VNC) or virtual non-calcium images, which are of interest in diagnostic radiology (74, 77, 78). Moreover, the spatial distribution of tissue properties such as Z_{eff} and ED may be reconstructed which can be of interest both in radiotherapy planning and diagnostic radiology (85-89).

VMI can add value to a diagnostic investigation by offering the potential of improved visualization of tissues, iodine and pathology (90-92). In VMI, the estimated attenuation at a specific photon energy is shown, whereas in a conventional reconstruction the attenuation is averaged over the X-ray beam spectrum. The theoretical benefit of VMI is essentially based on the relationship of CS and PE in a certain tissue. For iodine and materials of high atomic number, low energy VMI are dominated by attenuation due to PE and high energy VMI are dominated by the attenuation caused by CS. In soft tissues and water, the attenuation is dominated by CS in the diagnostic energy range, however the PE component is larger in low energy VMI. Optimization of contrast is possible given that the overall attenuation of tissues or features changes differently with energy.

Due to the ability to remove iodine contrast staining with DECT it has been shown to better distinguish ischemia after endovascular thrombectomy (93, 94), and distinguish between extravasated contrast medium and intracerebral hemorrhage after both endovascular thrombectomy and intravenous thrombolysis alone (95, 96). VMI reconstructed from dual-energy CTA scans show superior image quality and improve the diagnostic assessment of intracranial vessels when compared to conventional reconstructions (97-99).

Recent studies show promising results using different DECT techniques for acute stroke imaging by enhancing visualization of edema (100-103) or by the use of VMI (104, 105). At the start of this thesis project, the role of VMI to detect early ischemic changes in patients with suspected anterior circulation large vessel occlusion stroke had not been established.

Figure 3. A dual-layer detector DECT system at Karolinska University Hospital. On the outside, conventional CT and DECT systems have a similar appearance.

1.5.1.2 Dual-layer detector CT

A dual-layer detector CT (DL-DECT) adds dual-energy information to any acquisition performed with 120 or 140 kVp, i.e. it is "always in dual-energy mode" (81, 106). Essentially, low-energy photons are captured by the upper detector layer, whereas the bottom layer predominately captures the high-energy photons, as shown in figure 4 (106, 107). Unlike several other DECT techniques, image acquisition is with full field-of-view and benefit from perfectly registered spatial data and therefore the possibility of basis decomposition in the projection domain (106, 107). Beam hardening artifact reduction is an intrinsic benefit of projection-based decomposition (74, 75). Consequently, intracranial

metal artifact reduction has been shown in VMIs across the energy range (108). In addition, anti-correlated noise reduction can be exploited (109), which has been shown to improve image quality by optimizing CNR in previous studies on both phantoms and patients (91, 110-112). Previous studies on DL-DECT VMI have indicated superior intracranial image quality compared to conventional polyenergetic image reconstructions (91, 110, 112). In addition, it has been suggested that radiation dose may be reduced in non-contrast brain scans (113).

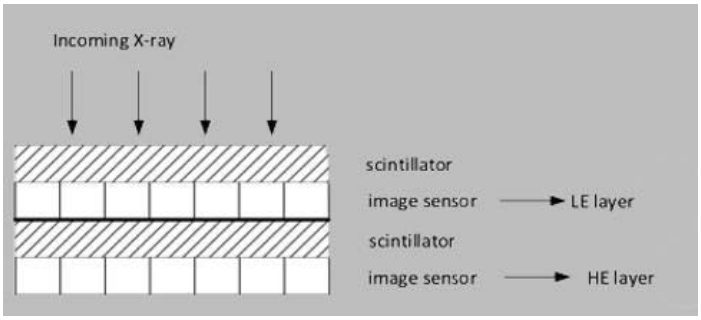

Figure 4. The concept of a dual-layer detector. Low-energy (LE) photons are registered in the top layer. The bottom layer captures the high energy (HE) photons.

1.5.2 Dual-energy cone-beam CT

Given the advantages described with DECT imaging in the previous section, employing photon energy spectrum separation in CBCT could generate energy and material selective images and thus improve tissue and iodine visualization. If a projection domain based reconstruction technique is employed (for example, using a dual-layer detector), it would also be possible to mitigate beam hardening artifacts and improve noise characteristics through anti-correlated noise reduction. This might improve the diagnostic properties of CBCT and increase its use in various clinical settings, including stroke imaging.

At the beginning of my doctoral studies, the most commonly used approach for studies on dual-energy CBCT (DE-CBCT) was temporal sequential scanning,

meaning two consecutive CBCT scans at low and high energy (114-117). This technique improved image quality and therefore also the accuracy of CBCT-based radiotherapy dose calculation (114, 116, 117). Evidently, sequential scanning is inconvenient as it results in increased acquisition time, with an increased risk of patient motion artifacts (118). In the setting of interventional radiology, rapid kV-switching DE-CBCT has been demonstrated, with disadvantages related to the speed of detector signal decay, as well as requiring a large separation in tube voltages (119).

1.5.2.1 Dual-layer detector CBCT

The idea of a layered flat detector for DE-CBCT has been studied with megavoltage (MV) beams, and more recently a kV dual-layer DE-CBCT (DL-DE-CBCT) flat detector prototype was described (120, 121). In kV DL-DE-CBCT, successful basis material decomposition and VMI reconstructions were performed (121).

Currently, there are no interventional C-arm systems capable of separating photon energy spectra in one rotational CBCT acquisition. Such a system, based on a dual-layer detector with the benefit of projection domain image reconstruction, would have the potential to acquire a diagnostic CBCT of improved quality in a multitude of clinical settings. In the setting of suspected LVO stroke, a sufficiently diagnostic CBCT acquisition in the interventional suite could replace CT, saving time, resources and have the potential of improved patient functional outcome (60, 70). As addressed in previous sections, material selective DE-CBCT reconstructions would also enable separation of blood from iodine, which is important when assessing complications after ischemic stroke treatment (95, 96). Moreover, improved tissue characterization would have potential utility outside stroke diagnosis and treatment, such as in adaptive radiotherapy (118).

1.6 Patient outcome

Treatment impact on patient functional outcome is of paramount importance. Selecting the most beneficial treatment for a patient can be challenging. Determination of tissue with irreversible damage (infarct) and regions with impaired oxygenation at risk of irreversible damage (penumbra) in relation to unaffected brain tissue gives important insight of brain integrity in the acute stroke phase. Infarct core volume assessed on non-contrast CT alone does not seem to predict patient outcome (122), however it has been shown that information from dynamic imaging (such as CTP), about ischemia and penumbra extent and localization, correlates to patient outcome (123). This justifies the rationale of diagnostic perfusion imaging performed before decision on treatment strategy in many of the large thrombectomy studies (16, 19, 20, 22, 23).

Although perfusion imaging may seem important, the necessity of it for patient outcome prediction has been discussed and possible alternatives have been addressed. As mentioned in previous sections, it has been shown that mCTA predicts tissue fate similarly to CTP (44) and even that single phase CTA collateral scoring may suffice for patient outcome prediction (124), obviating the need for mCTA and CTP for certain patients.

1.6.1 Time to treatment

Despite advancements of innovative imaging techniques and in the treatment of ischemic stroke, time management for patients potentially eligible for thrombectomy may be improved (125, 126). When the patient arrives at the hospital, he/she typically must first be transported to the CT scanner for diagnosis and then further to the interventional suite for thrombectomy. This consumes time and resources, and it is estimated that about 2 million neurons are lost per minute during an acute ischemic stroke caused by a large vessel occlusion (127). Consequently, a delay to efficient treatment may lead to additional manifest brain ischemia and poorer functional outcome (128). In

recent years, the concept of stroke diagnosis and treatment in the interventional angiography suite has been proven feasible in single-center studies, minimizing time to recanalization of occluded intracranial arteries (59, 70, 126).

2 Thesis overview

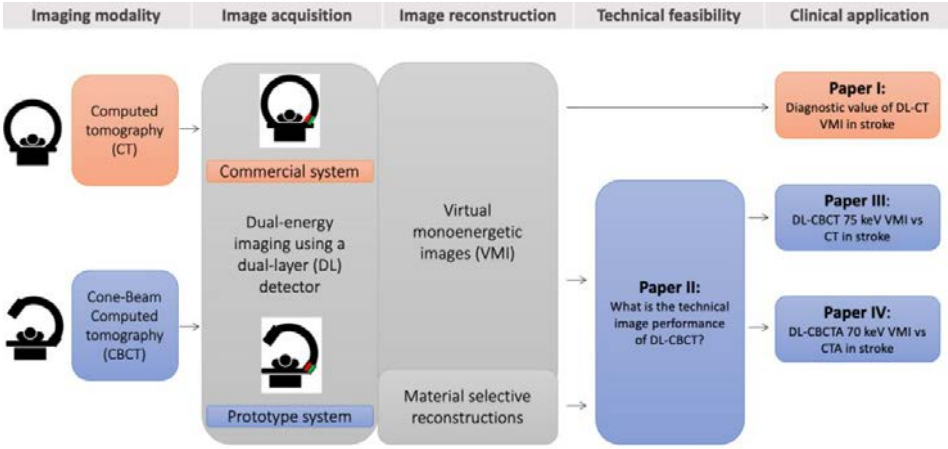

Figure 5. A visualization of the papers included in this thesis and their relationship to each other, with a brief description. DL-CBCTA = Dual-layer CBCT angiography, CTA = CT angiography.

3 Research aims

The overarching aim of this doctoral thesis was to study the utility and feasibility of dual-energy imaging in acute stroke (**paper I-IV**). The majority of the work presented is dedicated to a prototype dual-layer detector cone-beam CT (DL-CBCT) system (**paper II-IV**).

Given the theoretical benefits of improved image quality in dual-energy imaging, we first explored how virtual monoenergetic images (VMI) impact the identification of early ischemic changes in the brain using a commercially available imaging technique: non-contrast dual-layer dual-energy CT (**paper I**).

In **paper II,** we characterized a prototype DL-CBCT C-arm system with respect to technical performance through phantom studies.

In **paper III and IV**, we evaluated the performance of the prototype DL-CBCT system in stroke patients. Specifically, we studied the diagnostic accuracy of non-contrast DL-CBCT 75 keV VMI compared to CT in **paper III.** In **paper IV**, we studied the performance of intravenous DL-CBCTA 70 keV VMI compared to CTA. For both **paper III and IV**, We hypothesized that VMI DL-CBCT/A is sufficient for stroke diagnosis in the interventional suite.

Accordingly, we aimed to answer these research questions:

I. What is the diagnostic performance of automated ASPECTS in 40 – 120 keV VMI images compared to conventional CT?
II. How does the prototype DL-CBCT system perform with respect to technical image quality metrics, based on reconstructed images of phantoms?
III. Is non-contrast DL-CBCT 75 keV VMI non-inferior to non-contrast CT with regards to hemorrhage detection and ASPECTS accuracy?
IV. Is DL-CBCTA 70 keV VMI non-inferior to CTA with regards to arterial vessel visibility?

4 Materials and methods

4.1 Overview

	Paper			
Characteristic	I	II	III	IV
Data collection	Retrospective	Prospective	Prospective	Prospective
Design	Cohort	-	Cohort	Cohort
Participants	Human	Phantom	Human	Human
Image modality, reconstruction	DL-CT Non-contrast 40-120 keV VMI	DL-CBCT Conventional, VMI, material characterization	DL-CBCT Non-contrast 75 keV VMI	DL-CBCT 70 keV VMI angiography
Reference standard modality, reconstruction	CT Non-contrast conventional images	CBCT, DL-CT Conventional, VMI, material selective	CT Non-contrast conventional images	CT Conventional angiography
Patients studied	24	-	27	21
Inclusion period	Nov 2018 – July 2019	Feb 2020 - Feb 2021	Nov 2020 – Apr 2021	Nov 2020 – Apr 2021
Endpoints	Automated ASPECTS accuracy	Characterize MTF, noise, uniformity, Z_{eff}, ED, iodine quantification, VNC, CNR, CT number	Hemorrhage and ASPECTS accuracy, subjective image quality, CNR, SNR, noise, artifacts	Vessel visibility, artifacts

Table 1. Overview of the papers included in this thesis. As the dual-layer design implies dual-energy capability, the abbreviation used henceforth is DL-CT and DL-CBCT instead of DL-DECT and DL-DE-CBCT.

4.2 Paper I

4.2.1 Population

This retrospective single-center study included adult patients presenting with acute ischemic stroke caused by an occlusion of the intracranial internal carotid artery or proximal middle cerebral artery. Patients with previous stroke in the anterior circulation were excluded. Data was gathered on consecutive patients admitted to our institution between November 2018 and July 2019 who underwent initial diagnostic stroke imaging with DL-CT (IQon Spectral CT, Philips Healthcare, the Netherlands) and a subsequent routine follow-up CT one to three days after admission.

4.2.2 Image reconstruction

Conventional polyenergetic image reconstructions and VMI reconstructions at levels of 40 to 120 keV increments of 5 keV between 40 and 80 keV and in increments of 10–20 keV between 80 and 120 keV were obtained and reconstructed with 5 mm slice thickness. The conventional polyenergetic image reconstructions were performed per clinical routine and used for routine diagnostic workup.

4.2.3 Image analysis

In an attempt to limit interrater variability and bias, DL-CT conventional and VMI reconstructions were analyzed with an automated ASPECTS software (e-ASPECTS, v8.0, Brainomix Limited, Oxford, UK). DL-CT conventional reconstructions and routine follow-up CT were analyzed by three experienced stroke radiology raters to determine a reference standard ASPECTS (refASPECTS). Similar to a previous study validating the performance of e-ASPECTS (32), refASPECTS was defined as lesions present on both initial imaging

and follow-up CT. This meant that infarcts visible only on follow-up CT were not included in refASPECTS, as they could have developed after the initial scan. Consequently, the refASPECTS was not variable to treatment outcome. Only lesions identified by a majority of readers (i.e. two out of three) were included. Readers analyzed the images independently and were blinded to all information except the laterality of neurological symptoms, attempting to mimic the clinical setting of a stroke neuroradiologist. As the readers were not blinded to symptom laterality, 10 unilateral ASPECTS regions (in the hemisphere contralateral to patient symptoms) were evaluated per patient: four regions at ganglionic level (Caudate nucleus, Lentiform nucleus, Internal capsule and Insula) and six cortical regions (M1–M6).

4.2.4 Data analysis

Performance of conventional and VMI automated ASPECTS in relation to refASPECTS was analyzed using R statistical software (v3.6.3, The R Foundation for Statistical Computing). Region-based results of the automated ASPECTS conventional and VMI reconstructions were compared to refASPECTS to determine the true positive, false positive, true negative and false negative performance rate. Sensitivity, specificity, accuracy, negative predictive value and positive predictive value of each automated ASPECTS result was calculated. A 95% confidence interval (CI) was used to evaluate significance. For sensitivity and specificity, the CIs were adjusted by a ratio estimator (129), as the region-based analysis involved multiple (clustered) observations within each patient. If the number of positive or negative observations were six or below, the Wilson CI was used (130). For predictive values, the standard logit CI was calculated (131). Moreover, score-based error of conventional and VMI automated ASPECTS compared to refASPECTS was assessed by Bland-Altman plots.

4.3 Paper II

In this paper, several image properties of a prototype DL-CBCT C-arm system were evaluated with respect to reconstructed image performance.

4.3.1 System modification

Experiments in this study were made with a non-commercial prototype DL-CBCT system (Allura NEXIS Investigational Device, Philips Healthcare, The Netherlands, shown in figure 6). The DL-CBCT system is a modification of a commercial interventional C-arm X-ray system with CBCT imaging capability (Allura Xper FD20/15, Philips Healthcare, The Netherlands). Instead of the standard single-layer detector, the prototype is equipped with a dual-layer 20 inch non-CE marked detector. In essence, the prototype detector consists of two detector layers stacked on top of each other. Each layer consists of a flat detector based on a cesium iodide scintillator (see figure 4 for a schematic drawing).

4.3.2 Performance indicators evaluated

As a baseline indication of detector spatial resolution and image noise, the modulation transfer function (MTF) and image noise of the top layer standard reconstruction of the prototype was compared to a clinically available single detector layer CBCT C-arm system (Allura Xper FD20/15, Philips Healthcare, The Netherlands). Noise and uniformity characteristics of the updated top and bottom layer images ("front layer" and "combined layer" reconstructions as well as reconstructions of VNC and a multitude of VMIs) were then characterized. Material attribution feasibility was assessed by evaluating the accuracy of estimates of effective atomic number (Z_{eff}) and electron density (ED). Finally, the potential clinical advantages of the DL-CBCT were explored by quantifying the contrast-to-noise ratio (CNR) and CT number accuracy of relevant tissue substitutes, and assessing the performance in quantifying and suppressing iodine by means of iodine maps and VNC images.

Figure 6. The prototype DL-CBCT C-arm system (Allura NEXIS Investigational Device, Philips Healthcare, The Netherlands), on the outside practically identical to the commercial single detector layer CBCT C-arm system (Allura Xper FD20/15, Philips Healthcare, The Netherlands).

4.3.3 Phantoms

A Catphan CTP528 module (The Phantom Laboratory, Greenwich, NY, USA) containing line bars and spherical beads was used to assess the MTF. A cylindrical 19 cm diameter water phantom with plastic casing was used to evaluate CT-number uniformity and noise. Both phantoms were positioned in scan isocenter, suspended at the base and hanging free in air (see figure 7 A and B). The head module of the multi energy CT phantom model 662 (CIRS, Norfolk, VA, USA) was used to evaluate the attenuation of different inserts equivalent to various tissues, blood and iodine concentrations. This phantom was positioned at the scan isocenter, suspended by a carbon head rest over the table, simulating the position of a head scan (see figure 7 C).

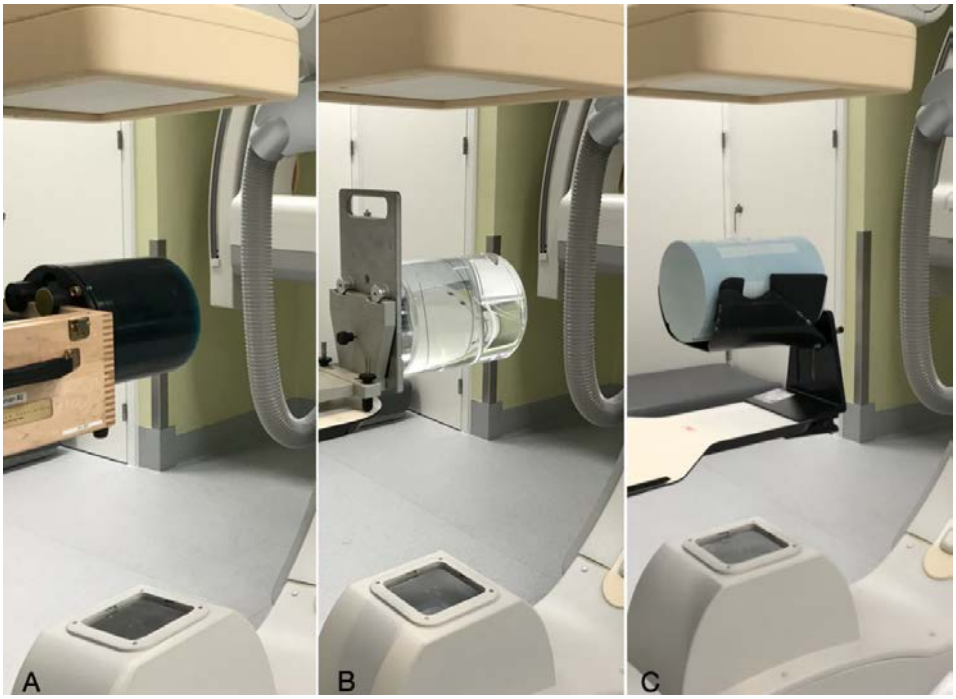

Figure 7. Setups of the different experiments. MTF measurements (A), water measurements (B) and multi energy phantom measurements (C).

4.3.4 Image reconstruction

Both non-spectral and spectral images were generated from the DL-CBCT scans. Virtual monoenergetic (VMI), iodine map, VNC, Z_{eff} and ED images were derived from material-decomposed Compton scatter and photo electric base functions in the projection domain (84). Noise suppression was realized as an optional step by exploiting the anti-correlated noise behavior after material decomposition (109). When used, noise suppression was applied to the material base images such that the noise in the VMI image at 70 keV matched that of a combined layer reconstruction. This was close to the fluence-weighted mean photon energy of the incident beam, 68 keV, determined using the SpekPy spectrum model (132). Since the denoising was done on the material base images and all other images are derived ones, all spectral images benefited from the denoising.

4.3.5 Data collection and analysis

Data collection was made with the ROI manager in ImageJ (U. S. National Institutes of Health, Bethesda, MD, USA) for all metrics except MTF which was collected using an automated software (Smári, The Phantom Laboratory, Greenwich, NY, USA). See figure 8 for an axial slice of ROIs used in the water phantom and multi energy phantom. The calculated CT numbers were obtained using the batch-specific elemental compositions and densities of the tissue substitutes as specified by the manufacturer. The National Institute of Standards and Technology (NIST) XCOM database was used to calculate the linear attenuation coefficients (133). Specific details about the collection of data variables for the various metrics are described in paper II. Normally distributed data was presented as mean with standard deviations.

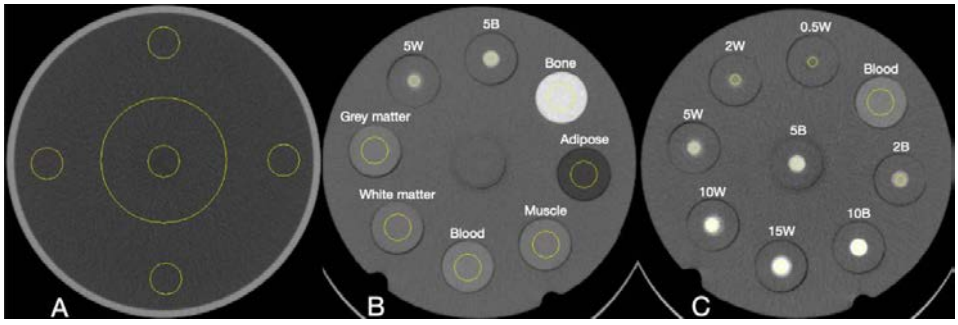

Figure 8. Virtual monoenergetic images at 70 keV with ROI placements. Water phantom (A), tissue equivalent inserts in multi energy phantom (B), iodine and blood equivalent inserts in multi energy phantom (C). Slice thickness 0.66 mm, window level 50, window width 500.

4.4 Paper III & IV

4.4.1 Study design and participants

The Next Generation X-ray Imaging System (NEXIS) trial was a single-center prospective cohort study conducted at a comprehensive stroke center (Clinicaltrials.gov identifier: NCT04571099). Patients with symptoms suggestive of an acute anterior circulation large vessel occlusion were triaged directly to the comprehensive stroke center as per clinical routine (134). Participants aged 50 years or older with ischemic stroke of the anterior circulation or hemorrhagic stroke were consecutively enrolled during office hours November 2020 – April 2021, after signing an informed consent. Initial imaging was performed according to clinical routine, typically including a non-contrast CT of the brain, multiphase CT angiography and CT perfusion. Depending on eligibility criteria, participants were imaged with non-contrast DL-CBCT and a single phase intravenous DL-CBCT angiography (DL-CBCTA) in an adjacent room once or twice (the same day as initial CT or/and one day after initial CT). If the participant was imaged with DL-CBCT/A one day after initial CT, it was done in conjunction with a follow-up non-contrast CT. A flow diagram of study participation is presented in figure 9. The DL-CBCT system (Allura NEXIS Investigational Device, Philips Healthcare) was a commercial interventional C-arm X-ray system (Allura Xper FD20/15, Philips Healthcare) fitted with a dual-layer 20 inch non-CE marked detector prototype, as described in paper II.

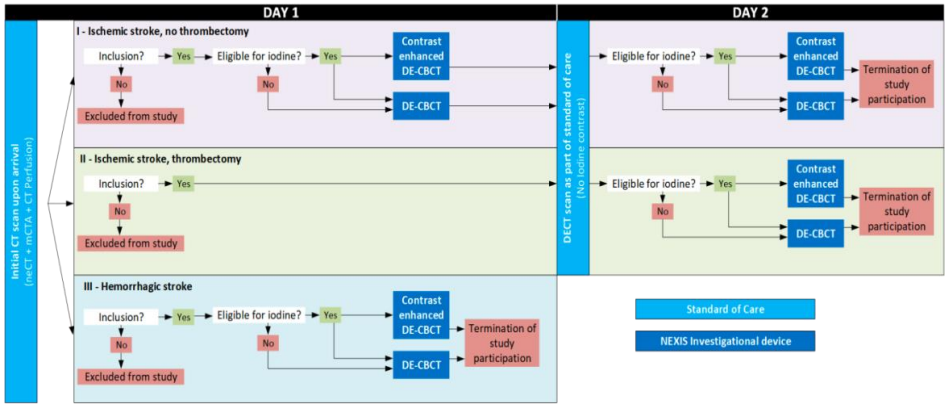

Figure 9. Schematic representation of the inclusion groups in a flow diagram. DE-CBCT = Dual-layer cone-beam CT, DECT= Dual-energy CT, neCT = Non-contrast CT, mCTA = multiphase CT angiography.

4.4.2 Image acquisition and reconstruction

Identical acquisition parameters were used in paper III and IV. In paper IV, all DL-CBCTA and CTA scans were with the same automated injection protocol: 85 ml of iodine 320 mg I/ml (Visipaque, GE Healthcare) 5 ml/s into a peripheral vein followed by a 80 ml saline chaser. The second phase CTA standard reconstruction was included in the study as reference standard, as it was reconstructed with a smaller field of view and the timing was typically more similar to the DL-CBCTA contrast phase (late arterial/arteriovenous). As described in paper II, DL-CBCT/A VMI images were derived from Compton and photoelectric base functions (basis material decomposition was performed in the projection domain) (84). Also, anti-correlated noise reduction was exploited as an inherent benefit of DL-CBCT/A (109).

4.4.3 Image analysis

Blinded pilot studies were performed by expert readers to determine the optimal VMI energy (50-90 keV) and noise reduction levels (three different levels) for stroke evaluation in the DL-CBCT/A images. Accordingly, DL-CBCT 75 keV VMI (paper III) and DL-CBCTA 70 keV VMI (paper IV) were selected with

moderate denoising level. Together with reference standard CT/A the images were randomized and evaluated independently by three neuroradiologists. Images were presented one modality at a time in a single-sequence, two-period crossover design with a mean washout period of 4 weeks (range 2–8 weeks). Readers were blinded to modality and there was no clinical information, such as symptom lateralization. A dedicated study software was used which allowed changes in slice thickness, viewing plane, window level and window width.

4.4.3.1 Assessment for pathology (paper III)

In paper III, the presence of hemorrhage and ASPECTS infarcts were evaluated on DL-CBCT. The corresponding CT result constituted the reference standard, as judged by the individual reader. In addition to individual reader results, the majority analysis is also presented, i.e. hemorrhage or infarcts according to at least 2 out of 3 readers.

4.4.3.2 Subjective image quality (paper III and IV)

In paper III, discrimination between gray and white matter was subjectively assessed in 17 supra- and infratentorial brain regions (ASPECTS regions and brain regions typically affected by artifacts) using 5-point Likert scales (5: Excellent, fully diagnostic, 1: None, uncertain for diagnosis). The perception of intracranial structures and artifact presence were assessed in 26 brain areas, including CSF spaces and brain stem in addition to the abovementioned regions (5: Excellent structure perception/No artifacts, 1: Structure not visible/Extensive artifacts, diagnostic evaluation impossible).

In paper IV, vessel visibility and artifact presence were evaluated separately as indicators of diagnostic quality on 5-point Likert scales, adopted with slight modifications from previous studies (5: excellent vessel visibility or no artifacts, 1: vessel not visible or extensive artifacts) (69, 135). Sixteen intracranial arterial segments were prospectively defined for the reader study. For the powered

analysis, some arterial segments were merged to render eleven arterial segments per patient. The score difference between DL-CBCTA and CTA for each segment in each patient determined whether a segment was considered inferior, equal or superior. In addition to individual reader results, the majority analysis is presented, i.e. segment judged as superior/equal vs inferior compared to CTA by at least 2 out of 3 readers.

4.4.3.3 Objective image quality (paper III)

In paper III, objective image quality was assessed by circular ROIs on 5 mm thick axial slices in the asymptomatic hemisphere, in accordance with previous studies on dual-energy CT of the brain (90-92). Noise, SNR and CNR for gray and white matter were determined using 25 mm^2 ROIs in two cortical locations and their juxtacortical white matter at the level of the basal ganglia, in the thalamus and the posterior limb of the internal capsule. To assess the impact of artifacts one 25 mm^2 ROI was placed adjacent to the skull bone at the level of the basal ganglia (in the "subcalvarial space" (91)), and one 200 mm^2 ROI in the interpetrous region of the posterior fossa. ROIs were automatically matched to the identical position in DL-CBCT and CT (see figure 10).

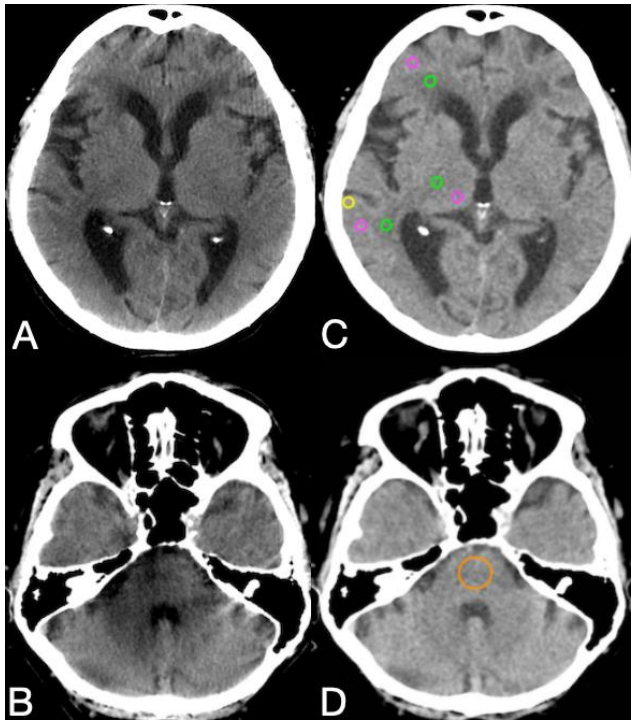

Figure 10. Axial non-contrast images of a participant with ischemic stroke. C–D show CT images with ROIs in the asymptomatic hemisphere and in the posterior fossa: gray matter (Magenta), adjacent white matter (Green), adjacent to the calvarium ("Subcalvarial", Yellow) and in the posterior fossa (Orange). ROIs were automatically matched to the identical position in the DL-CBCT 75 keV images (A–B). All W/L: 75/25, 5 mm slices with average intensity projection. DL-CBCT = Dual-layer cone-beam CT, ROI = Region of interest.

4.4.4 Statistical considerations

4.4.4.1 Sample size justifications

Sample size estimations aimed to prove diagnostic quality non-inferiority of DL-CBCT compared to CT according to three prospectively defined performance goals with thresholds for non-inferiority.

The sample size for the primary endpoint (presented in paper III) was trait-based, encompassing the 10 ASPECTS regions of the affected hemisphere in each participant. To evaluate the diagnostic accuracy of non-contrast DL-CBCT compared to reference standard CT, it was estimated that a sample size of 137

was required to render a power of 90% (target accuracy of 0.90, performance goal lower boundary of 0.80, one-sided alpha of 0.025). The lower boundary of the ASPECTS performance goal was set to not risk more than 20% false negatives or false positives (i.e. two ASPECTS areas). For this endpoint, a minimum sample size of 14 participants (140 regions) was required.

The 1st secondary endpoint was vessel tree visibility of DL-CBCTA (presented in paper IV). This endpoint was also trait-based, using 11 arterial segments for each participant. To evaluate the proportion of segments rated equal or superior to reference standard CTA, it was estimated that a sample size of 126 was required to render a power of 80% (target proportion of 0.90, performance goal lower boundary of 0.80, one-sided alpha of 0.0125, adjusted for multiple secondary endpoints). For this endpoint, a minimum sample size of 12 participants (132 segments) was required.

The 2nd secondary endpoint was diagnostic accuracy to determine the presence of intracranial hemorrhage (presented in paper III), comparing non-contrast DL-CBCT to reference standard CT. The endpoint was participant-based and it was estimated that a sample size of 20 was required to render a power greater than 95% (target accuracy of 0.9999, performance goal lower boundary of 0.80, one-sided alpha of 0.0125, adjusted for multiple secondary endpoints). The target for hemorrhage detection was set to not miss any bleeding given a limited number of participants. The estimated sample size included both participants with hemorrhage and negative controls, with a threshold of at least a 0.25 prevalence. For this endpoint, a minimum sample size of 20 was required.

In total, the minimum sample size required was estimated to 20 participants, of which two-thirds have ischemia, one-third have intracranial hemorrhage, and at least half must have done a DL-CBCTA. Our estimated necessary sample size was 29 subjects, taking optimizations and potential invalid data into account.

4.4.4.2 Statistical analyses

For the powered endpoints listed in the previous section, the exact binomial test with one-sided 98.75% confidence intervals (adjusted for multiple powered endpoints) was used, significance level $p<0.0125$. In paper IV, within-subject correlation of arterial segments was assessed by the Cochran-Mantel-Haenszel test (136).

In paper III, per-region ASPECTS agreement was assessed by the exact Fleiss Kappa, as it may be used for multiple readers, and reduces to the Cohens Kappa for two readers (137). The square weighted Cohens Kappa was used to assess the numerical ASPECTS agreement between modalities to compare with the largest CT ASPECTS study to date (138). In paper IV, the interrater agreement was assessed by the Fleiss Kappa (139). Kappa values were interpreted as: 0.01-0.20 slight agreement, 0.21-0.40 fair agreement, 0.41-0.60 moderate agreement, 0.61-0.80 substantial agreement and 0.81-0.99 almost perfect agreement (140).

In paper III, the two-sided Wilcoxon signed-rank matched-pairs test and the two-sided paired t-test were used for subjective and objective image quality comparisons, respectively. Bonferroni correction was applied to all analyses of image quality, $p<0.05$ was considered significant. Statistical analyses were made in RStudio (v1.4.1103, The R Foundation for Statistical Computing).

4.5 Ethical considerations

Paper I involved retrospective analysis of image data. The study was approved by the national ethical review authority (Ethical permit 2019-01309). Informed consent was waived in view of the retrospective nature of the study and since all procedures were part of routine care. The collection of data did not affect the patient and the analyses were made on group level. No additional risks were posed to the patient. In addition, informed consent would not be possible for all subjects since several subjects were anticipated to be deceased by the time of study initiation (this could potentially lead to a selection bias).

Paper II involved only phantoms with no specific ethical considerations.

For **paper III and IV**, there was a need to study the diagnostic capabilities of the novel detector in a relevant patient population. In order to evaluate diagnostic image quality in the acute stroke setting, we included subjects with ischemic stroke of the anterior circulation coming to Karolinska University Hospital. As initial imaging (with CT or CBCT) must be able to identify or exclude intracranial hemorrhage, subjects with a hemorrhagic stroke were also included in the study. An additional contrast enhanced scan is relevant for all stroke patients to delineate the intracranial vessels in order to identify relevant pathology. Thus, the interventions imposed on study participants were additional imaging and intravenous iodine contrast agent administration. All subjects received standard protocol healthcare in addition to their participation in the study.

Subjects received an additional radiation dose compared to standard diagnostic protocol due to the additional image acquisition. However, the brain is quite insensitive to radiation exposure (weighting factor of 0.01 when calculating effective organ doses (141)), and sensitivity to stochastic radiation effects decreases with age (142). The great majority of stroke patients in Sweden are 65 years or older (143). To ensure that the risks of additional radiation were minimized, no subject under the age of 50 were included in the study. No gender specific safety considerations were identified for subjects aged 50 and over. However unlikely, women included in the study are asked about current pregnancy.

Usage of iodine contrast agents poses a small risk of contrast-induced acute kidney injury. We followed the Swedish national guidelines, recommending that the total amount of iodine (in grams) administered for a contrast enhanced scan should not exceed the calculated aGFR in mL/min (144), given that the patient has a sufficient renal clearance and does not have multiple risk factors. These measures ensured that the risks associated with iodine contrast agents were minimized.

Informed consent was collected after oral and written information about all aspects that were relevant to the subject's decision to participate. This included general information about the study, risks for the individual, contact details for more information, and invitation to participate in the study on a voluntary basis. The information stated that there was no direct benefit for the subject, but that their participation could benefit future patients with the same diagnosis. Since patient integrity was of high importance, it was not possible to obtain informed consent through a family member or two physician consent. The including physician judged whether the patient was capable of making an informed decision. Personal data were anonymized and handled according to applicable laws. Patients were able to retract their participation at any time.

We believed that the most important ethical consideration was the added radiation dose and how this was weighed against the potential benefit for future patients with the same condition. The study was designed to provide a proof of concept and, given satisfactory results, could have substantial impact on time to treatment for patients eligible for thrombectomy. If it would be possible to both diagnose and treat large vessel occlusion ischemic stroke in the same room, we would expect a significant reduction in neuron loss due to ischemia and thus potentially have a positive impact on patient outcome. Therefore, we found these studies justified. The studies were approved by the Swedish ethical review authority (Ethical permit 2020-04467). The prototype DL-CBCT system was approved by the Swedish Medical Products Agency (document number 5.1-2020-6325), in accordance with the Medical Device Directive (MDD), which was the applicable legislation at the time. An independent qualified research organization contracted by the sponsor monitored the study.

Moreover, Philips Healthcare was the formal sponsor of the study with direct liability for the prototype DL-CBCT system. As a vendor of interventional systems, their involvement introduces a conflict of interest. In order to preserve scientific integrity, representatives from Philips were not involved in the primary data collection, interpretation or presentation of the results. It should be noted

that technical advancements in the field of radiology typically involves parties with commercial interests at some level. Funding for papers II-IV was provided from the European Commission (Horizon 2020, NEXIS-project, grant number 780026), which limited the presence of financial conflicts for Karolinska-affiliated researchers. However, it should be noted that Karolinska University Hospital has a master research agreement with Philips Healthcare.

5 Results

5.1 Paper I

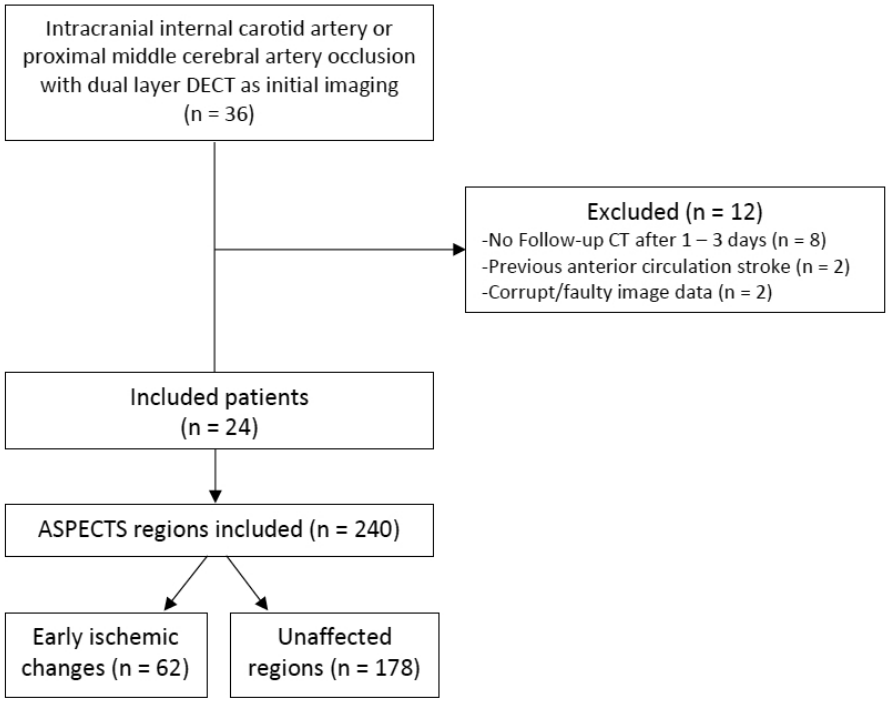

Figure 11. Flow diagram of screened subjects with intracranial internal carotid artery or proximal middle cerebral artery occlusion. Early ischemic changes and unaffected regions as defined by reference standard ASPECTS

5.1.1 Population

24 patients met the eligibility criteria, see figure 11. The median patient age was 75 and 50% were male. Median refASPECTS was 7 (interquartile range 6–8), and eighteen (75%) had a left sided occlusion.

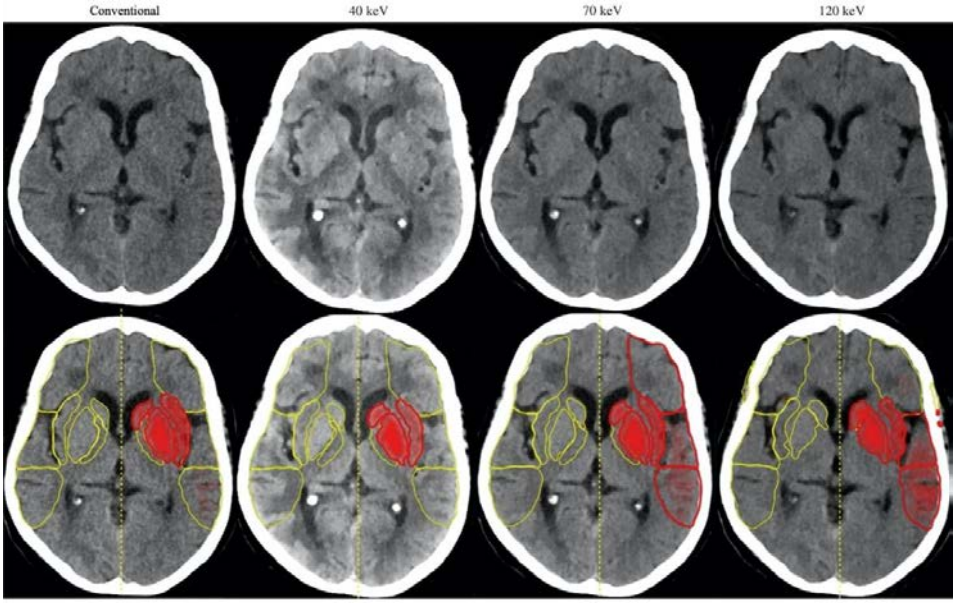

Figure 12. An example of axial image slices for conventional and VMI 40, 70 and 120 keV (from left to right) reconstructions. The second row shows the automated ASPECTS detection result, where red indicates an area with early ischemic changes. This patient had nine regions with early ischemic changes according to the refASPECTS (all except region M4), whereas the automated ASPECTS algorithm identified four regions in the conventional images, three in VMI 40 keV, eight in VMI 70 keV and eight in VMI 120 keV. refASPECTS = reference standard ASPECTS.

5.1.2 Diagnostic performance

62 regions with early ischemic changes were defined by refASPECTS (34 ganglionic and 28 cortical regions affected), and 178 unaffected regions (total n = 240 regions). Compared to refASPECTS, automated ASPECTS on conventional images showed a region-based accuracy of 0.89 (sensitivity 0.73 (95% CI 0.61–0.84), specificity 0.93 (0.91–0.98)). Of all image reconstructions, VMI 70 keV automated ASPECTS had the highest accuracy, 0.90 (sensitivity 0.82 (0.72–0.93), specificity 0.92 (0.88–0.97)), whereas VMI 40 keV had the lowest accuracy, 0.77 (sensitivity 0.34 (0.26–0.42), specificity 0.90 (0.89–0.96)). This pattern, showing highest accuracy for VMI 70 keV and lowest accuracy for VMI 40 keV, was also evident when evaluating ganglionic and cortical regions

separately. Figure 12 shows axial image slices for conventional and VMI 40, 70 and 120 keV reconstructions. Figure 13 visualizes the sensitivity and specificity for conventional and VMI automated ASPECTS at different energy levels of all regions, and separated into ganglionic and cortical regions.

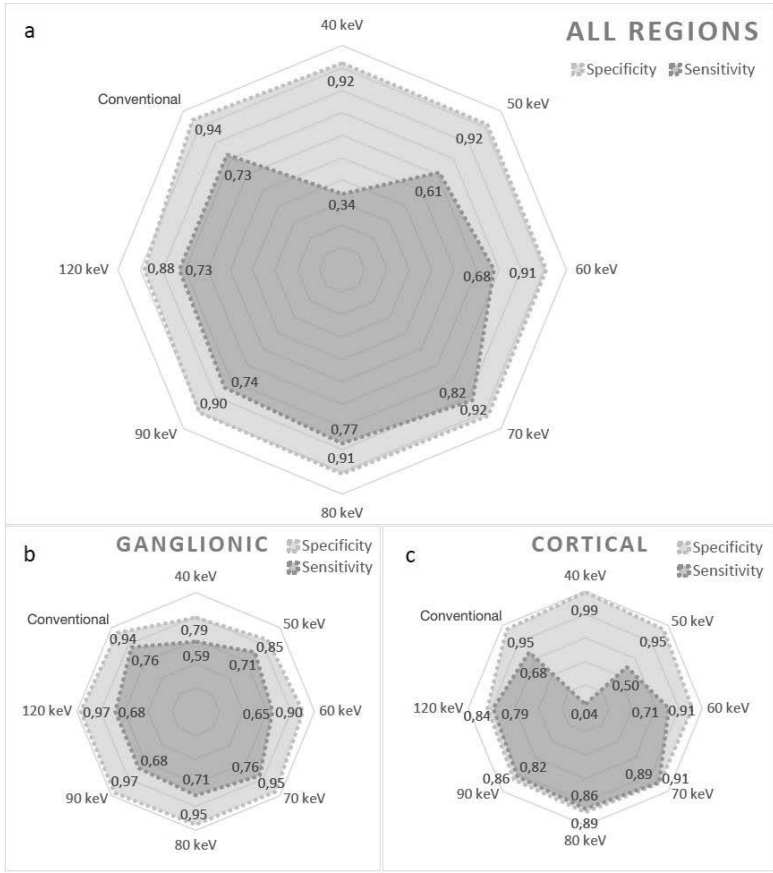

Figure 13. Visualization of the sensitivity and specificity for conventional and VMI automated ASPECTS at different energy levels of all regions combined (a), ganglionic (b) and cortical (c) regions.

All regions combined, the VMI 40 keV automated ASPECTS sensitivity 95% CI (0.26–0.42) did not overlap with any other automated ASPECTS sensitivity 95% CI. Moreover, the VMI 70 keV automated ASPECTS sensitivity 95% CI (0.72–0.93)

showed no overlap with VMI 40 or 50 keV sensitivity 95% CI (0.26–0.42 and 0.52–0.70, respectively). The difference in sensitivity for early ischemic changes appeared more distinct in cortical regions (95% CI 0.73–0.96 for VMI 70 keV, 0.01–0.18 for VMI 40 keV and 0.33–0.67 for VMI 50 keV automated ASPECTS, respectively). Interestingly, VMI 70 keV automated ASPECTS showed the highest negative predictive value of all reconstructions, 0.97 (0.92–0.99) for cortical regions and 0.94 (0.90–0.96) for all regions combined.

5.2 Paper II

5.2.1 Spatial resolution, noise and uniformity

The spatial resolution derived from the MTF curves was similar in the commercial and prototype systems using standard reconstruction software, as well as using the prototype reconstructions. Image noise levels were similar for the prototype and commercial system standard reconstructions, taking the differences in radiation dose into account. As mentioned in the methods, VMIs were noise matched to combined layer images at 70 keV and showed the highest noise level at 40 keV and the lowest at 80 keV. The least and most uniform VMIs were those reconstructed at 40 keV and 60 keV, respectively.

5.2.2 Material specific reconstructions

The mean image Z_{eff} relative to the estimated number was 98.2% (SD 1.2%) for all objects. The mean relative ED was 100.3% (SD 0.9%). For iodine quantification, images showed a mean difference of -0.1 (SD 0.5) mg/ml compared to the true iodine concentration for all blood and iodine containing objects. For VNC images, all blood substitutes containing iodine averaged a CT number of 43.2 (SD 3.3) whereas the blood-only substitute measured 44.8. On VNC, all water-containing iodine substitutes measured 2.6 (SD 2.9) in mean CT number. Figure 14 B-C displays sample images of the VNC and iodine map reconstructions, respectively.

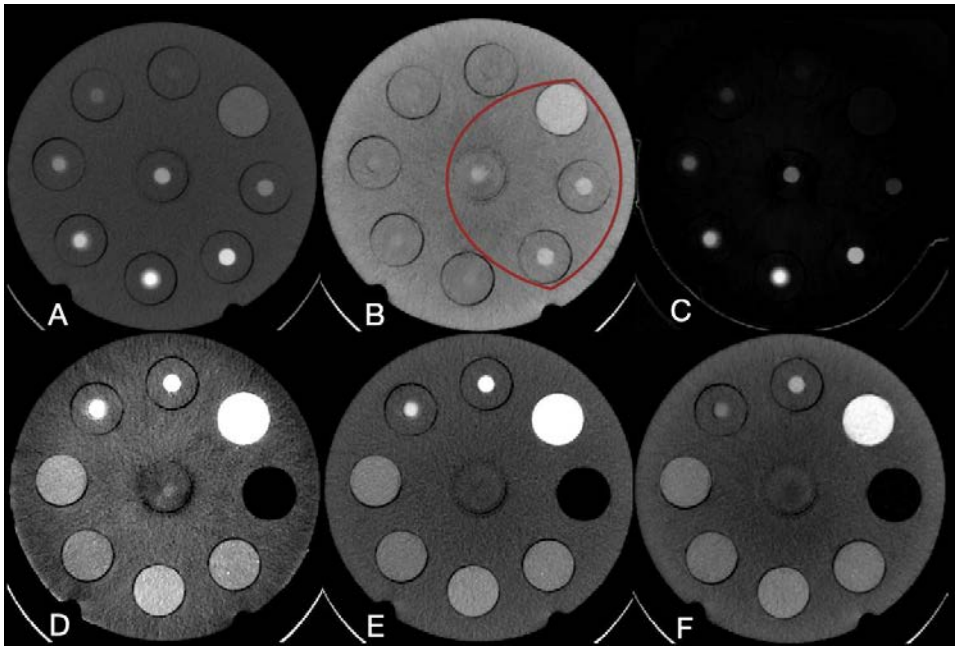

Figure 14. A–C: Phantom containing iodine inserts of different concentrations and a blood-only insert as shown in figure 8 C. D–F: Phantom with tissue equivalent inserts as depicted in figure 8 B. Slice thickness A–F is 0.66 mm. A: Virtual monoenergetic image (VMI) at 70 keV (window level (WL) 100, window width (WW) 400). B: Virtual non contrast image (WL 0, WW 200). The curved red line represents blood-containing inserts. These have a higher attenuation compared to the water-containing inserts. C: Iodine map (WL 7.5, WW 15). D–F: Image of VMI 40, 70 and 120 keV (all at WL 50, WW 200).

5.2.3 Contrast-to-noise ratio

Similar CNR patterns were seen across all studied tissue pairings: gray vs white matter, blood vs white matter and 5 mg/ml iodine in blood vs white matter. In the noise suppression matched dataset, front layer, combined layer and 70 keV VMI reconstructions had similar results, however 70 keV VMI had a tendency towards slightly higher CNR. In the same dataset, 40 keV VMI consistently had the highest CNR, and 120 keV had the lowest. Without noise suppression applied for the VMIs, a peak in CNR was seen at 70 keV VMI and a low at 120 keV VMI for all tissue pairings. See figure 15 for a graphical representation of the CNR of all tissue pairings.

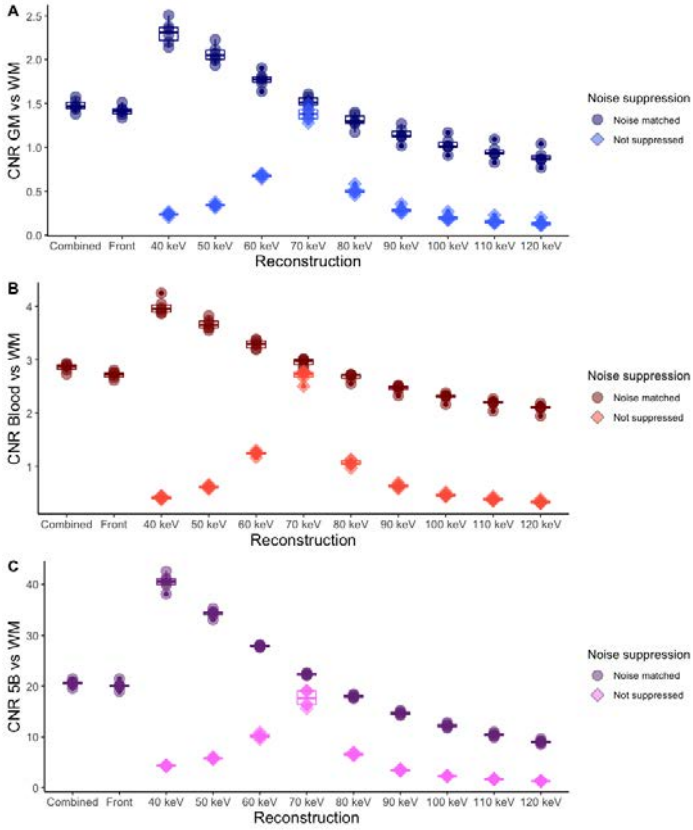

Figure 15. Contrast-to-noise ratio (CNR) characteristics from six repeat scans. Each dot represents the average value from six slices collected from each scan. Box plots are used to indicate the spread of the results. The noise suppression matched dataset (dark circles) and the dataset without noise suppression applied (bright diamonds) are shown. Data is presented for Gray matter vs White matter (A), Blood vs White matter (B) and Iodine in blood 5 mg/ml vs White matter (C).

5.2.4 CT number accuracy

Results for the reconstructed CT numbers of various clinically relevant objects in the VMI range of 40 – 120 keV are visualized in figure 16 A-C. Overall, the reconstructions are within or very close to the calculated CT number range (the range was defined as the tissue density uncertainty, estimated to be ±1%). At low

energies, the reconstructed CT numbers for some of the objects deviate by a few units of CT numbers from the expected trend.

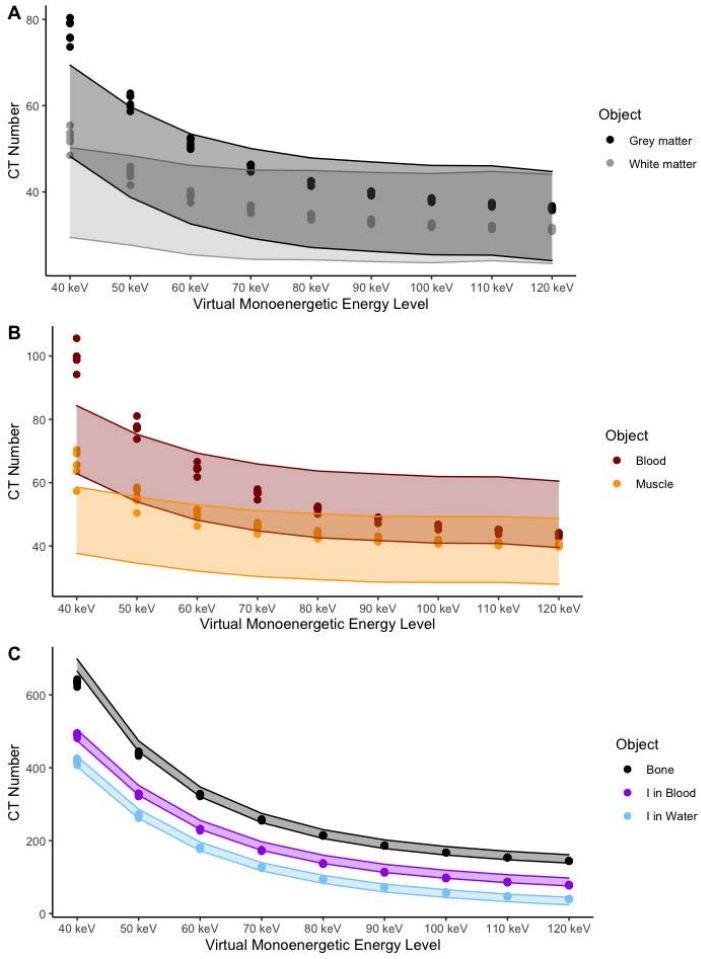

Figure 16. CT numbers of various clinically relevant objects in the virtual monoenergetic range of 40–120 keV from six repeat scans. Each dot represents the average value from six slices collected from each scan. The shaded ribbons marks the interval of the theoretical calculated CT number, with the limits being the CT number given an estimated tissue density uncertainty of ±1%. Bone= Bone 200 mg/ml; I in Blood= Iodine in blood 5 mg/ml; I in Water= Iodine in water 5 mg/ml.

5.3 Paper III

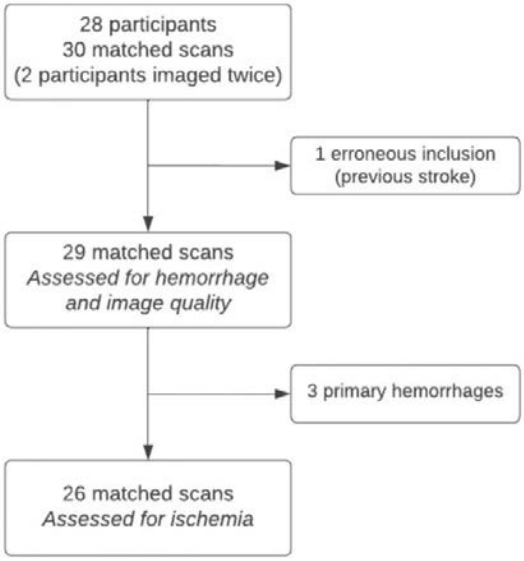

Figure 17. The flow diagram depicts which scans that were assessed for hemorrhage, image quality and ischemia, respectively.

5.3.1 Population

29 matched DL-CBCT and CT image sets from 27 prospectively enrolled participants were analyzed for hemorrhage identification and image quality assessment (see figure 17, flow diagram). 26 matched image sets from 24 participants were assessed for ischemic stroke, after excluding three participants presenting with hemorrhagic stroke. Mean age was 74 years ± 9, 19 were female (66%). The right hemisphere was affected in 17 participants (59%). Six scans (21%: 3 ischemic strokes, 3 hemorrhagic strokes) were performed on the day of symptom onset, the rest on day 2 (all ischemic stroke, post thrombectomy). Median time between CT and DL-CBCT was 17 minutes (IQR 12 – 28). Of the 26 scans used for ASPECTS region assessment, 24 (92%) presented with an occlusion of the intracranial internal carotid or proximal middle cerebral artery (M1 or M2 segment).

5.3.2 Hemorrhage detection

Three primary hemorrhages and five hemorrhagic transformations of ischemic stroke were detected in the reference CT examinations. Hence, eight matched scans with hemorrhages were included in the analysis (28% of all scans). Of these, two were small streaks of blood in the subarachnoid space. In the majority analysis, all eight hemorrhages were detected on DL-CBCT, 100% sensitivity and 100% specificity (100% accuracy, CI lower boundary 86%, p=0.002). One reader missed a small bleeding in the subarachnoid space on DL-CBCT, resulting in 88% sensitivity and 100% specificity (97% accuracy, CI lower boundary 80%, p=0.013) for the specific reader. There were no false positive hemorrhages.

5.3.3 ASPECTS assessment

In the per-region ASPECTS assessment (Figure 18), a higher accuracy was seen for all readers individually compared to the prospectively defined lower performance boundary of 80%. The lowest accuracy was seen for Reader 3: 86%, CI lower boundary 80%, p=0.010. Majority analysis showed 90% accuracy (CI lower boundary 85%, p<0.001). Sensitivity was 66% in the majority analysis, however readers individually performed slightly better compared to their individually defined reference standard CT (67, 69 and 76%, respectively). Specificity was 97% in the majority analysis (97%, 96% and 89% for each individual reader). Per-region Kappa was 0.49 for all readers (individually matched against each other 0.49, 0.42 and 0.54, respectively, all indicating moderate agreement)

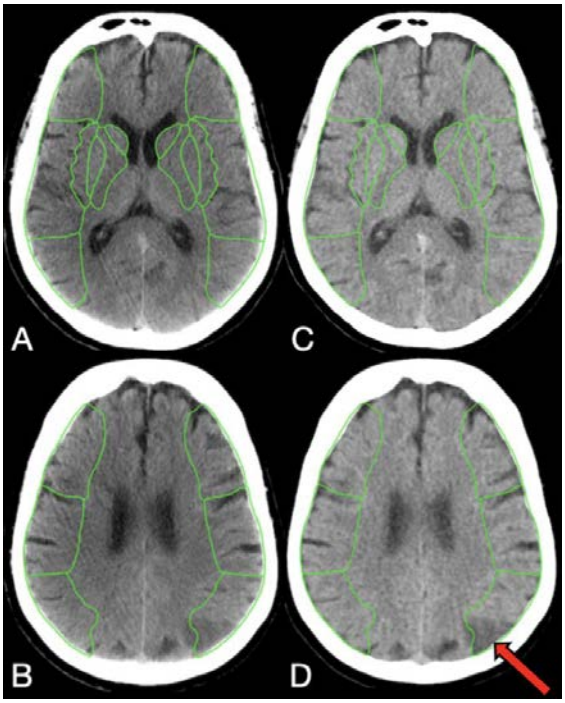

Figure 18. Axial non-contrast images of a participant with ischemic stroke. A–D shows ASPECTS regions boundaries at the level of the basal ganglia (A and C) and superior to the basal ganglia (B and D). A–B are DL-CBCT 75 keV images, C–D are CT images. There is an infarct in the left hemisphere M6 region (red arrow). All W/L: 75/25, 5 mm slices with average intensity projection. DL-CBCT = Dual-layer cone-beam CT.

Median CT ASPECTS was 9.5 (IQR 5–10) and DL-CBCT ASPECTS 9.5 (IQR 7–10) in the majority analysis. The most commonly infarcted region was the insula, followed by the lentiform nucleus, M2 and M5, and the least infarcted regions were the M1, M3 and M4. The weighted Cohens Kappa between the numerical CT and DL-CBCT ASPECTS was 0.59 (0.42 unweighted, both indicating moderate agreement).

5.3.4 Subjective and objective image quality

Averaged median Likert scores for gray and white matter differentiation, structure perception and artifacts for all regions were 3.0 in DL-CBCT, compared

to 4.0 or 4.3 for CT. Results were inferior to CT, p<0.001. When regions were analyzed separately, DL-CBCT showed significantly lower scores for each region individually, except for structure perception of the lateral ventricles.

For objective image quality, DL-CBCT showed a higher noise in all regions evaluated (p<0.001), lower SNR in gray and white matter (p<0.001), and a lower CNR between gray and white matter (p=0.006) compared to CT. The artifact indexes adjacent to the supratentorial skull bone ("subcalvarial") and in the posterior fossa were higher in DL-CBCT (p<0.001 and p=0.004), indicating a higher degree of beam hardening artifacts compared to CT.

5.4 Paper IV

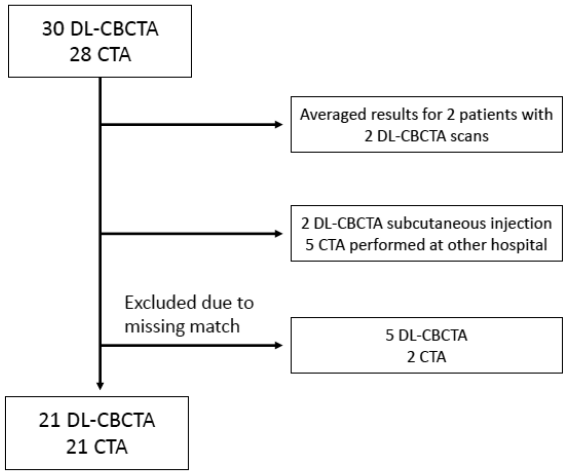

Figure 19. Of 28 consecutively enrolled patients, five had no in-house CTA and two were subject to subcutaneous intravenous contrast media injection during the DL-CBCTA scan. Two patients were imaged twice with DL-CBCTA, and the results from both scans were averaged. Consequently, 21 complete and matched DL-CBCTA and CTA image sets from 21 patients were included. DL-CBCTA = Dual-layer cone-beam CT angiography; CTA = CT angiography.

5.4.1 Population

21 matched DL-CBCTA and CTA image sets were included (Figure 19, flow diagram). Mean age was 72 years ± 9, fourteen were female (67%). The right hemisphere was affected in 11 (57%) patients. 3 patients had a hemorrhagic stroke. Of the remaining 18 patients with ischemic stroke, 17 (94%) presented with occlusion of the internal carotid or proximal middle cerebral artery (M1 or M2 segment) on CTA. In total, 17 patients (81%) were imaged with DL-CBCTA the day after CTA imaging (mean 23.8 hours ± 3.0). Four patients (19%) were imaged with DL-CBCTA on the same day as CTA (mean 1.2 hours ± 0.6 after CTA). Only the unaffected hemisphere was included in the statistical analysis.

5.4.2 Vessel visibility and artifacts

21 patients (231 matched arterial segments) were evaluated by each reader for the powered endpoint concerning overall arterial vessel visibility. One reader found non-inferior vessel visibility for DL-CBCTA in 90% of arterial segments (CI lower boundary 84%) and met the predefined non-inferiority criterium (lower performance boundary above 80%), whereas the two other readers did not, see the powered dataset with 231 segments in table 2. Majority analysis showed 77% of arterial segments rated non-inferior in DL-CBCTA (CI lower boundary 70%). Fleiss Kappa was 0.25 (Fair agreement).

Vessel Visibility	Powered dataset 231 segments	Powered subset 132 segments	Thrombectomy subset 132 segments
Majority	0.77 (0.70)	0.98 (0.93)*	0.98 (0.93)*
Reader 1	0.65 (0.58)	0.88 (0.80)*	0.91 (0.84)*
Reader 2	0.90 (0.84)*	0.98 (0.93)*	0.98 (0.93)*
Reader 3	0.60 (0.53)	0.78 (0.69)	0.88 (0.80)*

*Table 2. Proportion of DL-CBCTA arterial segment visibility rated equal or superior to CTA. Dataset (21 patients) include all scans, subset (12 patients) exclude poor scans. 98.75% CI of the one-sided lower performance boundary within brackets (lower boundary defined as 80% rated equal or superior). * indicates statistically significant result*

As 9 out of 21 (43%) DL-CBCTA scans were of poor quality due to patient motion or suboptimal timing of the contrast media injection (Figure 20), post-hoc analyses were also performed in a subset of 12 scans of acceptable quality. In the powered segment subset, the three readers found non-inferior vessel visibility in 98%, 88% and 78% of segments, respectively (two readers met the predefined performance goal). Majority analysis for non-inferiority was 98% (CI lower boundary 93%). Subsequently, 11 arterial segments especially relevant for thrombectomy candidates were selected for evaluation in the same patient subset (see the "thrombectomy" subset in table 2). Here, individual readers found non-inferior vessel visibility in 98%, 91% and 88% of segments, and all readers individually exceeded the CI lower performance boundary of 80% (Table 2). Fleiss Kappa was slightly higher compared to the powered dataset, 0.38 (Fair agreement). Regarding artifacts, non-inferiority was not seen in the full dataset or any subset analysis.

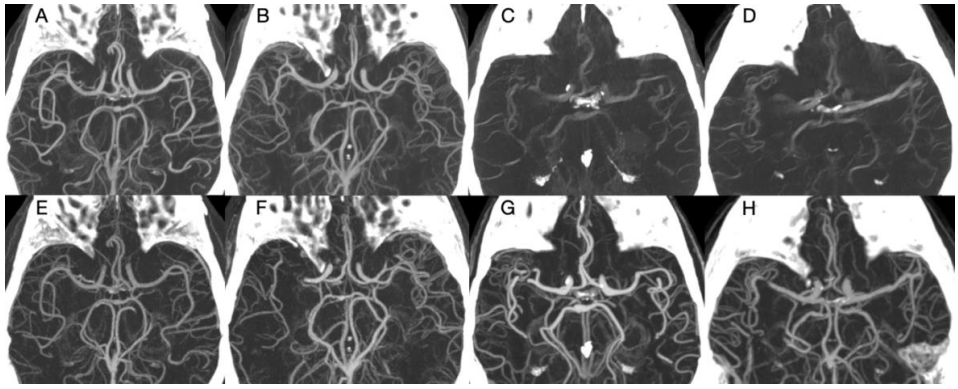

Figure 20. DL-CBCTA 70 keV images (top row) and CTA (bottom row) with MIP 35 mm slice thickness. A and B shows acceptable quality DL-CBCTA scans, while C and D shows typical scans in the dataset affected by motion artifacts. Bottom row (E to H) shows corresponding patient CTA. Note that images F, G and H show a right sided middle cerebral artery occlusion, which have been extracted at the time for DL-CBCTA imaging. Only the arteries in the unaffected hemisphere were evaluated. DL-CBCTA = Dual-layer cone-beam CT angiography; CTA = CT angiography; MIP = Maximum Intensity Projection

5.4.3 Analysis of individual segments

In the whole dataset, the A2-, M4- and AICA-segments vessel visibility were most commonly assessed as non-inferior (at least 76% for each reader and segment). The A2-segment was rated with least artifacts (majority 76% rated non-inferior), followed by A1-, M2-, M3-, M4-, P1- and P2-segments (majority 62 – 67% rated non-inferior). In the subset of acceptable scans, A2-, M4-, AICA- and P2- segments were most commonly rated as non-inferior (at least 92% for each reader and segment). In the subset majority analysis, 100% non-inferior vessel visibility was seen for all segments except M1 (75% rated non-inferior).

The lowest scores for vessel visibility were seen in the M1-segment, which was non-inferior to CTA in 57% of the whole dataset and in 75% of the subset in the majority analysis. The M1-segment also had a high degree of artifacts (only 43% rated non-inferior in the dataset and 67% in the subset). Similarly, the intracranial ICA-segment had a high prevalence of artifacts and among the lowest scores for vessel visibility in the dataset.

6 Discussion

First, a range of DL-CT VMI were explored in non-contrast scans with respect to their impact on automated detection of early ischemic changes. Second, a DL-CBCT prototype was evaluated with regards to reconstructed images through phantom experiments. Finally, using the DL-CBCT prototype, non-contrast VMI and VMI intravenous angiography were studied in a prospective human stroke cohort, with the hypothesis of non-inferiority compared to conventional CT.

6.1 Role of virtual monoenergetic images in stroke

In paper I, similar diagnostic accuracy in VMI levels of 60–120 keV automated ASPECTS was seen compared to automated ASPECTS in conventional images. In our study, 70 keV VMI automated ASPECTS had the highest sensitivity, accuracy and negative predictive value compared to reference standard. A high negative predictive value is important in the setting of acute ischemic stroke, where the presence of extensive ischemic damage impact clinical management and the presumed utility of thrombectomy. Accordingly, ASPECTS (≥6 or ≥7) has frequently been used as a fundamental eligibility criterion in the benchmark clinical trials studying the efficacy of endovascular stroke treatment (18, 19, 21, 22). Thus, our paper suggested 70 keV VMI automated ASPECTS as a feasible alternative to conventional reconstructions to exclude ischemic damage, particularly of cortical regions. Our findings were consistent with results of previous studies evaluating objective and subjective DECT image quality indices in brain scans with miscellaneous or no pathology (90, 91). Our results were in line with a concurrent study by van Ommen et al (105) where, dual-source DECT VMI reconstructions from 60 to 90 keV were the most sensitive and specific to identify early ischemic changes in patients with suspected ischemic stroke in the first phase of their study. As the second phase in the van Ommen study focused on infarct location match in both posterior and anterior territories, VMI 80–90 keV was ultimately designated as superior to identify infarcted brain

tissue, 80 keV being superior in the early time window. Their infarct location match essentially correspond to true positive results in five regions, of which only three are evaluated by ASPECTS. Rather, our study population was equivalent to the early time window subgroup studied, which constituted only about a third of the total study population in van Ommens study. These methodological differences, as well as our use of an automated detection algorithm and differences between DECT acquisition and reconstruction algorithms may account for our similar but not identical findings. Subsequently, Dodig et al, using a dual-source system, have found 80 keV VMI as the most valuable reconstruction for diagnosing ischemic stroke (145). Most recently, Mellander et al concluded that VMI in combination with conventional images may improve quality and diagnostic ability in stroke imaging, using a DL-CT system (146). Thus our findings, similar to others, find a modest improvement in image quality in VMI in the mid energy range over conventional images.

As our findings indicated that 70 keV VMI is a favorable monoenergetic level to identify anterior circulation acute ischemic stroke, image noise and beam hardening effects are relevant to address. Previous studies using dual-source and fast kVp-switching techniques have shown 67–72 keV and 68–77 keV VMI to provide the lowest image noise (90, 147, 148). As DL-CT VMI reconstruction algorithms benefit from perfectly registered spatial data, images can be generated following material basis decomposition in the projection domain. This approach enables anti-correlated noise reduction across the VMI energy spectrum, which has been shown beneficial in several studies on both phantoms and patients, with lowest noise in the mid- to high energy spectrum (91, 110-112). In addition, due to projection domain material decomposition, beam hardening artifacts can be corrected for effectively in dual-layer VMI (74). Accordingly, a beneficial VMI energy level to identify early ischemic changes should yield an adequate CNR between the relevant structures, a low noise profile and minimal beam hardening artifacts. This may be a contributing reason for why VMI 70 keV and slightly higher keV yielded a higher sensitivity compared to conventional

images in paper I. This effect in mid- to higher energy keV seemed much due to the increased sensitivity in cortical structures (close to the skull bone). This may be an effect of reduced beam hardening artifacts close to the skull bone, the effect of which should be most evident in mid- to high energy keV.

Our findings suggest that low energy VMI (VMI 40 keV and less explicitly 50 keV) have a low sensitivity and accuracy to identify early ischemic changes, most evident in cortical regions. Possible explanations are prominent beam hardening artifacts near the skull bone, as well as inferior noise characteristics at low VMI keV levels (90, 91, 110). Our results are reinforced by van Ommen et al (105) and Dodig et al (145), showing inferior performance for VMI 40 and 50 keV. Moreover, it is our impression that gray and white matter separation appears more distinct regardless of brain tissue viability at low keV VMI. This could potentially mask ischemic changes, which is hazardous in the acute stroke setting.

6.2 Feasibility of dual-layer CBCT

In paper II, spatial resolution was similar to the commercial CBCT standard reconstruction and demonstrated reproducibility and consistency between scans. Noise suppression was applied so that VMI 70 keV images matched the noise level of the combined layer reconstruction, however the lowest noise was seen in 80 keV reconstructions. This was likely due to the absorption of photons in the phantom, resulting in the mean energy impinging on the front and combined layer detector estimated to be 75 keV and 78 keV (slightly higher than the incident beam mean energy 68 keV).

The prototype accuracy of material property estimation (Z_{eff} and ED) and iodine quantification, was on par with a previous study investigating the accuracy of a clinical DL-CT (87). Overall, the iodine quantification results were superior to previously reported results on sequential scanning DE-CBCT and DL-CBCT (121, 149). VNC images provided a consistent separation of blood and iodine, with a distinct separation of blood and water in the reconstructed image. The

importance of distinguishing between extravasated iodine contrast media and blood following stroke treatment has been emphasized in previous chapters (95, 96). VMIs without noise suppression indicated an optimal reconstruction in terms of CNR to be achieved at 70 keV, similar to a previous study on a DL-CBCT (121). The noise-matched VMIs showed an increase in CNR with decreasing energy. This demonstrated a potential to manipulate CNR through both VMI energy selection and by noise suppression. Similar CNR trends have been shown using a frequency-split approach for noise reduction in DECT VMI datasets (150). Moreover, accurate CT numbers were estimated from various clinically relevant materials across the energy spectrum. Consequently, our results suggested a possible utility in diagnostic radiology.

6.3 Non-contrast dual-layer CBCT in stroke

Paper III was a non-inferiority study which compared dual-layer CBCT to CT in the setting of acute stroke. In the majority analysis, all hemorrhages were identified (100% accuracy, one-sided CI lower boundary 86%, p=0.002), however one reader missed a minimal bleeding in the left Sylvian fissure (97% accuracy, CI lower boundary 80%, p=0.013). The ASPECTS accuracy non-inferiority performance goal was met for all readers individually and in the majority analysis (90%, one-sided CI lower boundary 85%, p<0.001). As expected, DL-CBCT showed significantly inferior image quality compared to CT in the subjective and objective analyses. The results suggest that DL-CBCT can be used in the setting of suspected stroke, despite an inferior image quality compared to CT.

In 2017, a retrospective study including 32 ischemic stroke patients reported only 0—25% sensitivity to identify acute ischemic changes with CBCT (61). Since then, two monocentric studies compared CBCT ASPECTS to CT ASPECTS in stroke patients (prospective) and on patients with varying pathologies (retrospective), and reported 71-85% sensitivity and 83-94% specificity (66, 67). One recent retrospective study on non-circular scan trajectory CBCT ("sine

spin") in patients with varying pathologies showed 73% sensitivity and 95% specificity in reporting ischemic lesions (151). The three latter studies did not present individual reader results and CBCT scans were typically done with several hours separation to CT. Paper III showed comparable results (66—76% sensitivity and 89—97% specificity), and was conducted solely on stroke patients with a median of 15 minutes between modalities. This indicates that DL-CBCT have a similar accuracy to assess ischemic changes compared to previous studies on CBCT in a cohort with only stroke patients and a short time separation to the reference standard.

Per-region and numerical ASPECTS assessments are known to be highly variable between expert readers (31, 138). In paper III there is moderate agreement in the per-region analysis, similar to the largest CT ASPECTS study to date (Kappa 0.42-0.54, compared to a mean per-region Kappa of 0.52 in the CT ASPECTS study (138)). Moreover, the agreement of numerical ASPECTS in DL-CBCT compared to CT is comparable to that between readers in the CT ASPECTS study (Unweighted/weighted Kappa 0.42/0.59 compared to 0.39/0.56 in (138)). The findings supports the notion that DL-CBCT could be used to assess ASPECTS with a similar variability to CT.

Three previous publications studied the detection of intracranial hemorrhages with CBCT. One, including 45 intracranial hemorrhages, showed almost perfect performance for intracerebral and intraventricular hemorrhages, but missed half of the subarachnoid hemorrhages (61). Another reported 95—100% sensitivity and 97—100% specificity for all hemorrhage types (66). A third study showed 93% sensitivity and 90% specificity, with subarachnoid hemorrhage being the most challenging diagnosis (151). These results are in line with our findings and indicate that parenchymal hemorrhages (which account for the majority of hemorrhagic strokes) are typically detected, but small subarachnoid hemorrhages remains a challenge for DL-CBCT and CBCT alike. The minimal hemorrhage missed by a reader in our study occurred after treatment of an

ischemic stroke. Recently, it was suggested that such subarachnoid findings are associated with inferior functional outcomes (152).

Although significantly inferior results for subjective and objective image quality, DL-CBCT interestingly showed a gray and white matter SNR and CNR similar to polyenergetic CT reconstructions at comparable dose levels 10 years ago (90). The median DL-CBCT score of 3 for gray and white matter separation, overall structure perception and artifacts indicated a "decent, diagnostic" image quality, an acceptable perception of structures and slight artifacts overall. The lowest scores were typically recorded close to skull bone and in the posterior fossa, likely related to beam hardening effects.

Recently, VNC CT was demonstrated non-inferior to conventional CT to diagnose early ischemic changes according to ASPECTS (153). Moreover, sequential scan DE-CBCT was recently shown feasible to provide separation between hemorrhage and iodine contrast in patients (154). In paper III, we did not study VNC images, however this could have been clinically meaningful as participants likely had diffuse iodine extravasation, as elaborated on in the methodological considerations.

6.4 Dual-layer CBCT angiography in stroke

In paper IV, many scans (43%) were of poor quality due to movement artifacts or contrast media injection issues. Only one reader found DL-CBCTA non-inferior to CTA in the complete powered dataset. In a subset analysis excluding the poor quality scans, two readers individually (and the following majority analysis) found DL-CBCTA non-inferior. When only studying arteries relevant for thrombectomy in the subset, all readers individually found DL-CBCTA non-inferior to CTA. Image artifacts were generally more prevalent in the DL-CBCTA images.

Moreover, our results indicated that vessels that are not influenced by skull base artifacts, such as M4-, A2- and P2 segments, may have superior visibility in DL-CBCTA compared to CTA. Since the systems had similar spatial resolution, this

may be credited to fundamental differences between the DL-CBCTA and conventional CTA reconstructions. DL-CBCTA VMI had a lower absolute noise (realized through anti-correlated noise reduction), and may be superior in mitigating beam hardening effects from iodinated vessels due to material decomposition in projection space (74, 84, 109). On the contrary, segments adjacent to the skull base (most evidently M1 but also intracranial ICA to some extent) showed an inferior visibility compared to CTA. Even though beam hardening effects are reduced by VMI, the findings were expected, as circular CBCT scans of the brain typically are highly affected by beam hardening at the level of the skull base (155). As the M1- or ICA-segment are typically involved in LVO stroke, future development should focus on improving visualization of these segments. Lately, novel X-ray tube and detector scan trajectories were introduced in interventional CBCT systems to improve intracranial image quality by reducing bone beam hardening artifacts from the skull (151, 155). The term "butterfly", "dual-axis" or "sine-spin" are used, depending on the manufacturer.

In paper IV, we chose to study 70 keV VMI with moderate noise reduction on the basis of pilot studies, as elaborated on in the methodological considerations. Previous studies on VMI CTA of the head and neck arteries have suggested 40-60 keV VMI as superior to conventional CTA (97-99). However, these studies typically pursue quantitative optimization in terms of CNR, with a limited evaluation of subjective image quality based on radiologist interpretation. Although increasing CNR can be important, especially if iodine dose reduction is warranted, it does not seem to correlate fully with perceived diagnostic quality in human readers in our experience (156). In paper IV, we normalized window settings in our pilot study to a previous publication on dual-energy CTA (157). However, the need to individualize window settings may limit adoption of VMI in CTA or CBCTA. Moreover, in patients eligible for thrombectomy, concurrent imaging of the cervical vasculature is of interest, however this was not studied within the scope of paper IV.

6.5 Technical considerations of the DL-CBCT prototype system

In paper II, there was an artifact present in the center of the image which degraded the uniformity metric and affected the potential clinical utility of the prototype system. The artifact was caused by a detector imperfection. Since paper II was an early prototype study, the artifact was reduced in the subsequent clinical studies.

The prototype scan time was 20 seconds to enable dual-layer image acquisition. In paper IV, 9 scans (43%) were considered to be of poor quality, predominantly due to patient motion artifacts. No systematic evaluation of movement artifacts were made for paper III, but our impression was that in paper IV, iodine contrast administration along with a longer patient time on the table may have influenced patient movement. In accordance with the study protocol and ethics approval, no repeat scans were made. A long scan time is a typical limitation of CBCT, which should be considered when selecting a suitable imaging modality for stroke patients. Typical scan times for current state-of-the-art CBCT acquisition protocols are 7-10 seconds (151, 155). It is important to minimize the risk of patient movement in awake patients with limited compliance. An improved head fixation may decrease motion artifacts (66). Moreover, new reconstruction methods may decrease the effects of patient motion in CBCT (158-160). Finally, some DL-CBCTA scans suffered from suboptimal iodine injection timing. Manual bolus tracking was not possible since we used a prototype system. Instead, a fixed injection delay protocol was used.

6.6 Methodological considerations

6.6.1 Paper I

Important limitations of this study was the retrospective nature, small sample size, single center and only using a single CT scanner. CT was used as the reference standard as diffusion weighted MRI is not part of the clinical routine. Moreover, VMI acquisition and reconstruction techniques vary between different

manufacturers and scanner type which affects the generalizability of the results (106).

The automated software for ASPECTS assessment was not explicitly intended to be used on VMI. Therefore, automated ASPECTS performance in VMI, especially in the low and high end of the energy spectrum, should be interpreted with caution. An automated detection algorithm removes inter-reader differences, factors related to personal taste and observer bias (review bias, insufficient blinding) and thus provides an efficient solution to conduct a study, however other biases are introduced related to limited datasets used for training (161).

6.6.2 Paper II

The detector performance was not isolated and characterized in paper II. Instead, the system performance was assessed in terms of reconstructed images. However, the parameters examined were properties commonly determined by quality control measurements (MTF, noise and uniformity) and relevant to clinical performance. The prototype results were also limited, based on a single scan protocol, with a phantom in isocenter. Nevertheless, these determinations of spatial resolution and noise indicate that the prototype DL-CBCT system generally matched the capabilities of current commercial systems, while proving dual-energy capabilities. The impact on performance from changes in protocol, setup and phantom warrants further investigation.

We demonstrated the ability to manipulate CNR through a suitable choice in VMI energy level for clinically relevant materials. This illustrated the potential utility in maximizing the visibility of anatomy or other relevant features. However, optimization in the clinical setting needs to consider the limitations of CNR as a indicator of detectability.

6.6.3 Paper III & IV

6.6.3.1 General considerations

In both papers, strengths included the prospectively defined endpoints, a clinically relevant study population and the assessment by blinded readers. Typically, outcomes in previous publications were not prospectively defined and not adjusted for multiple comparisons (62, 63, 68, 69).

Although it is difficult to specify clinically distinct non-inferiority margins, we sought to minimize the risk of type one error as elaborated on in the statistical considerations chapter (162). Limitations for both papers further included the single center study design and relatively small sample size. We powered the study based on traits, not patients, adding complexity as the exact binomial test ideally warrants independent data (163). Moreover, since the participants were recruited during office hours (the majority after thrombectomy had been performed) and needed to sign the informed consent themselves (not possible through family member or two physician consent), a selection bias was present. This resulted in a relatively small cohort and excluded the majority of patients with hyperacute or large infarcts in paper III.

In addition, papers III and IV did not explicitly study the optimum VMI for different clinical tasks. Instead, one energy and noise reduction level was chosen for each task on the basis of blinded pilot studies of perceived image quality. In paper III, the selection of 75 keV VMI for DL-CBCT was in line with paper I and previous studies both with regards to overall perceived intracranial image quality (90-92), and to the identification of ischemic stroke (105, 145). The selection of 70 keV VMI in paper IV has been discussed in a previous chapter. In both papers, the denoising level chosen was higher than the one used for noise matching in paper II, which reasonably contributed to a higher CNR.

Only one acquisition protocol was used in each study. A high kVp tube output theoretically reduces beam hardening artifacts caused by the skull bone, however visualization of iodinated vessels may benefit from a lower kVp (164). In

paper III and IV, we chose to use a single acquisition protocol at 120 kVp, as low kVps reduce the separation of photon energy spectra in a dual-layer detector design. Known challenges with a dual-layer detector include obtaining sufficient separation of photon energy spectra, which can be improved by using a filter material between the detector layers. We chose not to use a filter as this also decreases dose efficiency (106, 165). Adding complexity, the optimal VMI keV likely also depend on dual-energy technique and reconstruction kernel (92). In summary, optimization of acquisition and reconstruction parameters are warranted in future studies.

6.6.3.2 Paper III

In paper III, the majority of all scans were acquired one day after stroke symptom onset, after thrombectomy. As in paper I, CT was used as the reference standard since MRI was not part of clinical routine. Although progression of time typically facilitates the distinction of ischemic changes, diffuse intracranial iodine contrast staining (due to blood-brain barrier leakage after initial scans) may render the evaluation of ischemic changes more challenging (95). As CT and DL-CBCT were acquired with little separation in time, both modalities were equally affected by potential iodine contrast staining. ASPECTS scoring is known to be variable among readers, and in paper III we chose to score ASPECTS at the ganglionic and supraganglionic level in accordance with the original definition (31). This approach can omit information about ischemic changes in the adjacent ganglionic and supraganglionic territories. Only eight intracranial hemorrhages were studied, of which the majority were hemorrhagic transformations. This also limits the generalizability of our results.

6.6.3.3 Paper IV

In paper IV, non-symptomatic vessel segment visibility and artifacts were evaluated as properties of diagnostic quality. The study design and power

calculation intended to evaluate the diagnostic quality of the entire intracranial arterial vasculature. In the setting of LVO stroke, it may be advantageous to power a diagnostic study with regards only to large diameter arteries. However, this would miss information about collateral arteries and small concurrent occlusions. Powering the study with regards to participants would be a desirable alternative, however this implies a larger cohort. Readers were not specifically instructed on how to assess variant anatomy or perforating arteries, which likely affected interrater variability (Kappa results were only fair). Previously, CBCTA have been studied using a reconstructed image pixel matrix of 512 x 512, similar to CT (68). In paper IV, using a 384 x 384 pixel matrix impacts the level of detail and noise characteristics, which may affect the perception of image quality.

6.6.4 Dataset considerations (paper I & III)

The automated ASPECTS algorithm was blinded to patient symptom laterality, compared to the reference standard in paper I. As the automated ASPECTS consistently identified the correct affected hemisphere in our study, theoretically, 10 more true negatives could be added for each patient scan (i.e. for the unaffected, healthy hemisphere), evaluating 20 regions in total. Arguably, using only 10 ASPECTS regions is the most realistic approach in the context of LVO (one would rarely suspect an ipsilateral infarction when symptom laterality is known). Doing the contrary would add negative results, decrease infarct prevalence and thus skew the accuracy, specificity and negative predictive value of the study results. Notably, negative and positive predictive values are highly dependent on prevalence and should be interpreted with caution (166).

The above considerations are also valid in paper III, where only one hemisphere was taken into account in the statistical analysis, despite blinded readers. The measure of accuracy is also dependent on prevalence, which would have been negatively skewed, potentially introducing misleading results if additional negatives would have been added to the dataset (166). When interpreting and comparing diagnostic ability, it is important to consider whether the dataset is

representative for the relevant study population. Ultimately, careful consideration of sensitivity and specificity is important to understand the diagnostic utility of a new method (167). In paper I the prevalence of ischemic changes was about 26%, in paper III about 20%, which we considered representative for patients admitted in an early time window for the evaluation of a potential LVO. The lower prevalence in paper III is likely related to ethical aspects of prospective patient inclusion, as noted previously.

7 Conclusions

VMIs impact the identification of early ischemic changes on DL-CT. In a retrospective single-center DL-CT cohort, automated 70 keV VMI ASPECTS had the highest diagnostic accuracy, sensitivity and negative predictive value overall.

The DL-CBCT prototype system showed comparable spatial resolution and noise to a commercially available CBCT system, while offering dual-energy capability. The dual-energy images indicated a consistent ability to separate and characterize clinically relevant tissues, blood and iodine. Thus, the DL-CBCT system could find utility in the diagnostic setting.

Non-contrast DL-CBCT 75 keV VMI showed non-inferior hemorrhage detection and ASPECTS accuracy to CT in a prospective single-center stroke patient cohort. However, image quality was inferior compared to CT, and visualization of small subarachnoid hemorrhages after treatment remains a challenge.

In the same prospective single-center stroke patient cohort, DL-CBCTA 70 keV VMI showed non-inferior vessel visibility compared to CTA under certain conditions. Specifically, the prototype system had a long scan time and was not capable of bolus tracking which resulted in scan issues. After excluding participants with such issues, DL-CBCTA 70 keV VMI were found non-inferior to CTA.

In summary, the findings of this thesis indicate that DL-CBCT may be sufficient for stroke assessment in the interventional suite with the potential to bypass CT in patients eligible for thrombectomy. However, issues related to the prototype system and the visualization of small hemorrhages highlight the need of further development.

8 Points of perspective

Results from recent multicenter randomized clinical trials conducted in Asia, North America, Europe and Oceania published in 2022-2023 indicate favorable patient outcome in anterior circulation LVO patients presenting with large infarcts subjected to endovascular intervention (168-170). These trials included patients presenting with ASPECTS 3-5 (two trials also had perfusion imaging as alternative inclusion criteria) and last known well within 24 hours (one trial used 6 hours as cut-off). The results from these trials are likely to further strengthen the role of thrombectomy as the primary treatment for anterior circulation LVO. As ASPECTS can be evaluated on a non-contrast brain scan, the role of advanced imaging such as perfusion CT or multiphasic CTA is subject to discussion.

Arguably, these findings may reinforce the idea of transporting suspected LVO patients directly to the interventional suite for diagnostic work-up in order to reduce time to treatment. If at least some viable tissue remain (ASPECTS at least 3) and a LVO is ascertained, the patient may receive thrombectomy with conceivable benefit. Ongoing large trials are evaluating the feasibility and effect of primary diagnostic work-up with CBCT and subsequent treatment in the interventional room for LVO stroke patients. The global multicenter WE-TRUST randomized trial is evaluating the impact on workflow and patient outcome compared to CT/MRI (72). Recently, the multi-center SPINNERS trial with the primary purpose to investigate non-inferiority of intracranial hemorrhage detection in sine spin CBCT compared to CT was launched (171). If eligible, a patient not suited for thrombectomy may receive thrombolysis, provided that intracranial hemorrhage is excluded. As the option to give thrombolysis is fundamental in stroke treatment, this is likely a prerequisite for widespread implementation of a “direct to interventional suite” approach.

Energy-resolved X-ray imaging or “spectral imaging” are umbrella terms including dual-energy and more recently imaging achieved through energy-resolving X-ray detectors, photon counting detectors (PCD). Photon counting CT (PCCT) is an emerging technology with the potential of improved imaged quality,

added image information and reduction of radiation exposure (172). Although not addressed specifically in this thesis, the technique must be recognized as ground-breaking for medical X-ray imaging. PCDs utilize semiconductors instead of scintillator material (as used together with photo-diodes in traditional energy integrating detectors, EIDs) (172). Thus, instead of creating a light signal, photons directly generate an electric charge that is registered by the detector (direct-conversion). There are several advantages associated with PCDs. First, smaller detector pixels can be constructed without dose penalty since there is no longer a need for light-separating septa between detector pixels (otherwise used for scintillator material) (172, 173). Second, an energy detection threshold can be set to eliminate electronic noise, with a resulting increase in SNR and possibilities for dose reduction (172, 174). Third, the PCDs have intrinsic sensitivity for different photon energies. Individual pulse heights for incident photons can thus be measured and separated into different energy bins by thresholding, enabling multi-energy imaging (175). Fourth, the PCDs intrinsically weigh low- and high energy photons equally in the ideal scenario (one count for each photon), in contrast to EIDs where low-energy photons are weighted less relative to high-energy photons, as they contribute with less light signal. Since low energy photons typically carry more contrast information, there is a potential to increase CNR with PCDs (176). Relevant to brain imaging, PCCT have shown superior CNR in non-contrast VMIs compared to EID CT, and PCCT VMI angiography have indicated reduced in beam hardening artifacts in the skull base region (174, 177). Exploiting the inherent benefits listed above, there are multiple areas of potential clinical use, including improved resolution of anatomy, detectability and characterization of pathology.

Recently, the feasibility of high-quality volumetric PCD-CBCT with a C-arm system was shown and subsequently integrated into a hybrid PCD-scintillator flat detector design (178, 179). The pursuit of ultra-high resolution and improved tissue, blood, iodine and material characterization in the interventional room will continue to unfold in the coming years, with conceivable benefit to our future

patients. This thesis shows the potential of DL-CBCT to provide clinical benefit in the interim until PCD-CBCT technology has matured. Moreover, the strategies and study designs elucidated in this thesis provides a template for evaluating similar technology, including PCDs, in a pre-clinical and clinical setting.

9 Acknowledgements

First, my sincere gratitude to all study participants - you made this thesis possible. Next, I would like to thank the following people in particular:

My main supervisor **Anna Falk Delgado**. Thank you for investing your time and for believing in me. To me, you have been a role model for scientific curiosity, integrity and efficiency. Thank you for always making time, even on short notice. Among many things that I carry with me, you have emphasized the importance of always keeping an open mind and to seek new perspectives.

My co-supervisor **Gavin Poludniowski**. Thank you for your sharing your bright mind, your patience and kindness throughout these years. Thank you for being a great educator, and for being pertinent and exact. Thank you for always caring.

My co-supervisor **Staffan Holmin**. Thank you for finding ways to make good use of my interests, for providing an excellent research environment, and for always having an open door if I needed to discuss something.

Michael Söderman. You let me take the wheel and taught me how to steer. In many ways, you enabled this thesis. I am forever grateful to you!

Åke Holmberg. For working hard and for always having a strong opinion. And for showing me how to make a decent landstings-espresso.

Håkan Almqvist and **Artur Omar** – thank you**!** Håkan for taking me under your wings that first summer in 2017, for sparking my interest in stroke and for continuous collaboration ever since – always with a good story at hand. Artur for being there to sort out "the complicated stuff", with kindness and creativity.

Jens Kolloch, **Åsa Aspelin** and **Vamsi Gontu**. Thank you for being great and efficient collaborators as well as outstanding colleagues. Vamsi – special thanks for being the top dog on the racket court: losing builds character. Also, thank you **Odett Ghalamkari** for choosing dual-energy for your masters project!

Heidrun Steinhauser and **Ernst Hermens,** for successfully leading NEXIS with great enthusiasm and dedication. Thank you to the Horizon 2020 programme and all consortium members at Philips, KU Leuven, TU Eindhoven, Trixell, TNO, imec and 3DCeram. Without the combined efforts from all of you, this thesis would not have been possible. A special attention to my co-authors **Fred van Nijnatten**, **Paul Withagen**, **Axel Thran**, **Peter van de Haar**, **Bernd Menser** and **Klaus-Jürgen Engel** – thank you! **Marijke van Vlimmeren**, **Erik Hummel** and **Mathias Simon** – your efforts have been especially important to me and I hope that we may continue with exciting discoveries onwards. **Dirk Schäfer**, you

deserve a particular mention for your diligence, kindness and outstanding collaboration in many aspects of this thesis – and for crossing the Baltic sea in a kayak! Lastly, **Kevin Najarian**, thank you for great statistics input and discussions.

Michael Mazya, for your bright, kind and pragmatic mind. You have been a key collaborator throughout the clinical studies. Thanks to you and your colleagues at the Neurology department, we made it through the NEXIS clinical study.

A special mention to **Erik Fredenberg** and my mentor **Mats Danielsson**. Erik, for being a brilliant colleague at the inception of NEXIS, and Mats for always having an open door. Thank you both for being fun and inspiring people.

Thank you to my research groups – old and new! **Rikard**, **Arvin** and **Philip**, thank you for valuable discussions and perspectives as I embarked on my PhD, and **Francesca** and **Annika K** for being great colleagues in my "new home".

Thank you to all exceptional colleagues at the department of Neuroradiology, it is a great privilege to work with you! A special mention to **Fabian** for mentoring my clinical journey and for being a great inspiration. **Johanna & Johanna** for letting me play with the machines. **Magnus Kaijser** and **Babak Flahat**, for betting on me in the very beginning. Also **Jens Hultcrantz,** for co-surviving that first summer.

Thank you **Jiri Bartek Jr** and **Arvid Frostell** for fun and guidance in the early days. Thank you also to all colleagues at the Neurosurgical department for great collaboration over the years, including **Adrian Elmi-Terander** and **Erik Edström** both in clinic and later joint research. **Jonathan Nordblom** first introduced me to Staffan, so you are kind of guilty as well.

Thank you **Linn** and **Mateusz** for no fuss and lots of fun over the years.

Thank you **Gnekens Vänner** and everyone affiliated to this entity of friends. You know who you are and you mean a lot. May our joint memories fill another book.

Karin and **Per Damlin**, thank you for being fun and relaxed, and for providing a recreational playground, including hide & seek, joint adventures, and experiments by the grill. **Carl**, **Linnéa** and little **Helga** – hanging out together is so much fun!

My parents **Henia** and **Lasse**. Thank you for your unconditional love and support. You have always provided me with a close-knit sense of security, and inspiration when I needed it. My brother **Patrik**, you are the most caring and brilliant brother one could imagine. Thank you for always having my back. **Maja**, **Henry** and **Stella**, spending time with you fills me with joy – but how did you grow up so fast?!

My beloved **Anna**. You mean more to me than words can describe. Thank you for being my rock, my cloud nine and my ever shining sun. You complete me.

10 References

1. Johnson W, Onuma O, Owolabi M, Sachdev S. Stroke: a global response is needed. Bull World Health Organ. 2016;94(9):634-a.
2. Feigin VL, Forouzanfar MH, Krishnamurthi R, Mensah GA, Connor M, Bennett DA, et al. Global and regional burden of stroke during 1990-2010: findings from the Global Burden of Disease Study 2010. Lancet. 2014;383(9913):245-54.
3. WHO Global Health Estimates 2019. Geneva: The World Health Organization; 2020.
4. Virani SS, Alonso A, Benjamin EJ, Bittencourt MS, Callaway CW, Carson AP, et al. Heart Disease and Stroke Statistics—2020 Update: A Report From the American Heart Association. Circulation. 2020;141(9):e139-e596.
5. WHO. Preventing chronic diseases: a vital investment Geneva, Switzerland: World Health Organization; 2005 [
6. Feigin VL, Lawes CM, Bennett DA, Barker-Collo SL, Parag V. Worldwide stroke incidence and early case fatality reported in 56 population-based studies: a systematic review. Lancet Neurol. 2009;8(4):355-69.
7. Johnston SC, Mendis S, Mathers CD. Global variation in stroke burden and mortality: estimates from monitoring, surveillance, and modelling. Lancet Neurol. 2009;8(4):345-54.
8. Patel A, Berdunov V, Quayyum Z, King D, Knapp M, Wittenberg R. Estimated societal costs of stroke in the UK based on a discrete event simulation. Age and Ageing. 2020;49(2):270-6.
9. Tsao CW, Aday AW, Almarzooq ZI, Anderson CAM, Arora P, Avery CL, et al. Heart Disease and Stroke Statistics—2023 Update: A Report From the American Heart Association. Circulation. 2023;147(8):e93-e621.
10. Riedel CH, Zimmermann P, Jensen-Kondering U, Stingele R, Deuschl G, Jansen O. The importance of size: successful recanalization by intravenous thrombolysis in acute anterior stroke depends on thrombus length. Stroke. 2011;42(6):1775-7.
11. Molina CA, Montaner J, Abilleira S, Ibarra B, Romero F, Arenillas JF, et al. Timing of Spontaneous Recanalization and Risk of Hemorrhagic Transformation in Acute Cardioembolic Stroke. Stroke. 2001;32(5):1079-84.
12. Ullberg T, Andersson T. Reperfusionsbehandling vid akut stroke har lett till paradigmskifte. Lakartidningen. 2023;120.
13. Tissue Plasminogen Activator for Acute Ischemic Stroke. New England Journal of Medicine. 1995;333(24):1581-8.
14. Hacke W, Kaste M, Bluhmki E, Brozman M, Dávalos A, Guidetti D, et al. Thrombolysis with Alteplase 3 to 4.5 Hours after Acute Ischemic Stroke. New England Journal of Medicine. 2008;359(13):1317-29.
15. Campbell BCV, Ma H, Ringleb PA, Parsons MW, Churilov L, Bendszus M, et al. Extending thrombolysis to 4.5-9 h and wake-up stroke using perfusion imaging: a

systematic review and meta-analysis of individual patient data. Lancet (London, England). 2019;394(10193):139-47.

16. Goyal M, Menon BK, van Zwam WH, Dippel DW, Mitchell PJ, Demchuk AM, et al. Endovascular thrombectomy after large-vessel ischaemic stroke: a meta-analysis of individual patient data from five randomised trials. Lancet (London, England). 2016;387(10029):1723-31.

17. Berkhemer OA, Fransen PS, Beumer D, van den Berg LA, Lingsma HF, Yoo AJ, et al. A randomized trial of intraarterial treatment for acute ischemic stroke. N Engl J Med. 2015;372(1):11-20.

18. Jovin TG, Chamorro A, Cobo E, de Miquel MA, Molina CA, Rovira A, et al. Thrombectomy within 8 hours after symptom onset in ischemic stroke. N Engl J Med. 2015;372(24):2296-306.

19. Saver JL, Goyal M, Bonafe A, Diener HC, Levy EI, Pereira VM, et al. Stent-retriever thrombectomy after intravenous t-PA vs. t-PA alone in stroke. N Engl J Med. 2015;372(24):2285-95.

20. Campbell BC, Mitchell PJ, Kleinig TJ, Dewey HM, Churilov L, Yassi N, et al. Endovascular therapy for ischemic stroke with perfusion-imaging selection. N Engl J Med. 2015;372(11):1009-18.

21. Goyal M, Demchuk AM, Menon BK, Eesa M, Rempel JL, Thornton J, et al. Randomized assessment of rapid endovascular treatment of ischemic stroke. N Engl J Med. 2015;372(11):1019-30.

22. Albers GW, Marks MP, Kemp S, Christensen S, Tsai JP, Ortega-Gutierrez S, et al. Thrombectomy for Stroke at 6 to 16 Hours with Selection by Perfusion Imaging. N Engl J Med. 2018;378(8):708-18.

23. Nogueira RG, Jadhav AP, Haussen DC, Bonafe A, Budzik RF, Bhuva P, et al. Thrombectomy 6 to 24 Hours after Stroke with a Mismatch between Deficit and Infarct. N Engl J Med. 2018;378(1):11-21.

24. Hounsfield GN. Computerized transverse axial scanning (tomography): Part 1. Description of system. The British Journal of Radiology. 1973;46(552):1016-22.

25. Kalender WA. Computed tomography: fundamentals, system technology, image quality, applications: John Wiley & Sons; 2011.

26. OECD. Computed Tomography scanners per million inhabitants: OECD.Stat; 2021 [Available from: https://stats.oecd.org/index.aspx?queryid=30184.

27. Hounsfield GN. Computed medical imaging. Nobel lecture, Decemberr 8, 1979. Journal of computer assisted tomography. 1980;4(5):665-74.

28. Levi C, Gray JE, McCullough EC, Hattery RR. The unreliability of CT numbers as absolute values. AJR Am J Roentgenol. 1982;139(3):443-7.

29. Kjos BO, Brant-Zawadzki M, Young RG. Early CT findings of global central nervous system hypoperfusion. AJR Am J Roentgenol. 1983;141(6):1227-32.

30. Barber PA, Demchuk AM, Zhang J, Buchan AM. Validity and reliability of a quantitative computed tomography score in predicting outcome of hyperacute

stroke before thrombolytic therapy. ASPECTS Study Group. Alberta Stroke Programme Early CT Score. Lancet. 2000;355(9216):1670-4.

31. Pexman JH, Barber PA, Hill MD, Sevick RJ, Demchuk AM, Hudon ME, et al. Use of the Alberta Stroke Program Early CT Score (ASPECTS) for assessing CT scans in patients with acute stroke. AJNR American journal of neuroradiology. 2001;22(8):1534-42.

32. Nagel S, Sinha D, Day D, Reith W, Chapot R, Papanagiotou P, et al. e-ASPECTS software is non-inferior to neuroradiologists in applying the ASPECT score to computed tomography scans of acute ischemic stroke patients. Int J Stroke. 2017;12(6):615-22.

33. Herweh C, Ringleb PA, Rauch G, Gerry S, Behrens L, Mohlenbruch M, et al. Performance of e-ASPECTS software in comparison to that of stroke physicians on assessing CT scans of acute ischemic stroke patients. Int J Stroke. 2016;11(4):438-45.

34. Pfaff J, Herweh C, Schieber S, Schonenberger S, Bosel J, Ringleb PA, et al. e-ASPECTS Correlates with and Is Predictive of Outcome after Mechanical Thrombectomy. AJNR Am J Neuroradiol. 2017;38(8):1594-9.

35. Olive-Gadea M, Martins N, Boned S, Carvajal J, Moreno MJ, Muchada M, et al. Baseline ASPECTS and e-ASPECTS Correlation with Infarct Volume and Functional Outcome in Patients Undergoing Mechanical Thrombectomy. J Neuroimaging. 2019;29(2):198-202.

36. Albers GW, Lansberg MG, Kemp S, Tsai JP, Lavori P, Christensen S, et al. A multicenter randomized controlled trial of endovascular therapy following imaging evaluation for ischemic stroke (DEFUSE 3). Int J Stroke. 2017;12(8):896-905.

37. Leslie-Mazwi T, Chandra RV, Baxter BW, Arthur AS, Hussain MS, Singh IP, et al. ELVO: an operational definition. Journal of NeuroInterventional Surgery. 2018;10(6):507.

38. Demeestere J, Wouters A, Christensen S, Lemmens R, Lansberg MG. Review of Perfusion Imaging in Acute Ischemic Stroke. Stroke. 2020;51(3):1017-24.

39. Koopman MS, Berkhemer OA, Geuskens R, Emmer BJ, van Walderveen MAA, Jenniskens SFM, et al. Comparison of three commonly used CT perfusion software packages in patients with acute ischemic stroke. Journal of neurointerventional surgery. 2019.

40. García-Tornel Á, Campos D, Rubiera M, Boned S, Olivé-Gadea M, Requena M, et al. Ischemic Core Overestimation on Computed Tomography Perfusion. Stroke.0(0):STROKEAHA.120.031800.

41. Ma H, Campbell BCV, Parsons MW, Churilov L, Levi CR, Hsu C, et al. Thrombolysis Guided by Perfusion Imaging up to 9 Hours after Onset of Stroke. N Engl J Med. 2019;380(19):1795-803.

42. Garcia-Tornel A, Carvalho V, Boned S, Flores A, Rodriguez-Luna D, Pagola J, et al. Improving the Evaluation of Collateral Circulation by Multiphase Computed Tomography Angiography in Acute Stroke Patients Treated with Endovascular Reperfusion Therapies. Interv Neurol. 2016;5(3-4):209-17.

43. Menon BK, d'Esterre CD, Qazi EM, Almekhlafi M, Hahn L, Demchuk AM, et al. Multiphase CT Angiography: A New Tool for the Imaging Triage of Patients with Acute Ischemic Stroke. Radiology. 2015;275(2):510-20.

44. d'Esterre CD, Trivedi A, Pordeli P, Boesen M, Patil S, Hwan Ahn S, et al. Regional Comparison of Multiphase Computed Tomographic Angiography and Computed Tomographic Perfusion for Prediction of Tissue Fate in Ischemic Stroke. Stroke. 2017;48(4):939-45.

45. Pierot L, Jayaraman MV, Szikora I, Hirsch JA, Baxter B, Miyachi S, et al. Standards of practice in acute ischemic stroke intervention: International recommendations. Interv Neuroradiol. 2019;25(1):31-7.

46. Jaffray DA, Siewerdsen JH. Cone-beam computed tomography with a flat-panel imager: initial performance characterization. Med Phys. 2000;27(6):1311-23.

47. Parker DL. Optimal short scan convolution reconstruction for fanbeam CT. Med Phys. 1982;9(2):254-7.

48. Doerfler A, Golitz P, Engelhorn T, Kloska S, Struffert T. Flat-Panel Computed Tomography (DYNA-CT) in Neuroradiology. From High-Resolution Imaging of Implants to One-Stop-Shopping for Acute Stroke. Clin Neuroradiol. 2015;25 Suppl 2:291-7.

49. Dijkstra ML, Eagleton MJ, Greenberg RK, Mastracci T, Hernandez A. Intraoperative C-arm cone-beam computed tomography in fenestrated/branched aortic endografting. J Vasc Surg. 2011;53(3):583-90.

50. Tacher V, Radaelli A, Lin M, Geschwind J-F. How I Do It: Cone-Beam CT during Transarterial Chemoembolization for Liver Cancer. Radiology. 2015;274(2):320-34.

51. Soderman M, Babic D, Holmin S, Andersson T. Brain imaging with a flat detector C-arm : Technique and clinical interest of XperCT. Neuroradiology. 2008;50(10):863-8.

52. Sepúlveda I, Schmidt T, Platín E. Use of cone beam computed tomography in the diagnosis of superior semicircular canal dehiscence. J Clin Imaging Sci. 2014;4:49.

53. Güldner C, Diogo I, Bernd E, Dräger S, Mandapathil M, Teymoortash A, et al. Visualization of anatomy in normal and pathologic middle ears by cone beam CT. Eur Arch Otorhinolaryngol. 2017;274(2):737-42.

54. Venkatesh E, Elluru SV. Cone beam computed tomography: basics and applications in dentistry. J Istanb Univ Fac Dent. 2017;51(3 Suppl 1):S102-s21.

55. Siewerdsen JH, Jaffray DA. Cone-beam computed tomography with a flat-panel imager: magnitude and effects of x-ray scatter. Med Phys. 2001;28(2):220-31.

56. Nagarajappa AK, Dwivedi N, Tiwari R. Artifacts: The downturn of CBCT image. J Int Soc Prev Community Dent. 2015;5(6):440-5.

57. Miracle AC, Mukherji SK. Conebeam CT of the Head and Neck, Part 1: Physical Principles. American Journal of Neuroradiology. 2009;30(6):1088-95.

58. Razi T, Niknami M, Alavi Ghazani F. Relationship between Hounsfield Unit in CT Scan and Gray Scale in CBCT. J Dent Res Dent Clin Dent Prospects. 2014;8(2):107-10.

59. Psychogios MN, Behme D, Schregel K, Tsogkas I, Maier IL, Leyhe JR, et al. One-Stop Management of Acute Stroke Patients: Minimizing Door-to-Reperfusion Times. Stroke. 2017;48(11):3152-5.

60. Psychogios MN, Maier IL, Tsogkas I, Hesse AC, Brehm A, Behme D, et al. One-Stop Management of 230 Consecutive Acute Stroke Patients: Report of Procedural Times and Clinical Outcome. J Clin Med. 2019;8(12).

61. Eckert M, Golitz P, Lucking H, Struffert T, Knossalla F, Doerfler A. Optimized Flat-Detector CT in Stroke Imaging: Ready for First-Line Use? Cerebrovascular diseases (Basel, Switzerland). 2017;43(1-2):9-16.

62. Struffert T, Deuerling-Zheng Y, Kloska S, Engelhorn T, Strother CM, Kalender WA, et al. Flat detector CT in the evaluation of brain parenchyma, intracranial vasculature, and cerebral blood volume: a pilot study in patients with acute symptoms of cerebral ischemia. AJNR American journal of neuroradiology. 2010;31(8):1462-9.

63. Struffert T, Deuerling-Zheng Y, Kloska S, Engelhorn T, Lang S, Mennecke A, et al. Dynamic Angiography and Perfusion Imaging Using Flat Detector CT in the Angiography Suite: A Pilot Study in Patients with Acute Middle Cerebral Artery Occlusions. AJNR American journal of neuroradiology. 2015;36(10):1964-70.

64. Psychogios MN, Buhk JH, Schramm P, Xyda A, Mohr A, Knauth M. Feasibility of angiographic CT in peri-interventional diagnostic imaging: a comparative study with multidetector CT. AJNR American journal of neuroradiology. 2010;31(7):1226-31.

65. Nicholson P, Cancelliere NM, Bracken J, Hummel E, van Nijnatten F, Withagen P, et al. Novel flat-panel cone-beam CT compared to multi-detector CT for assessment of acute ischemic stroke: A prospective study. European Journal of Radiology. 2021;138:109645.

66. Leyhe JR, Tsogkas I, Hesse AC, Behme D, Schregel K, Papageorgiou I, et al. Latest generation of flat detector CT as a peri-interventional diagnostic tool: a comparative study with multidetector CT. Journal of neurointerventional surgery. 2017;9(12):1253-7.

67. Maier IL, Leyhe JR, Tsogkas I, Behme D, Schregel K, Knauth M, et al. Diagnosing Early Ischemic Changes with the Latest-Generation Flat Detector CT: A Comparative Study with Multidetector CT. AJNR American journal of neuroradiology. 2018;39(5):881-6.

68. Saake M, Breuer L, Goelitz P, Ott S, Struffert T, Doerfler A. Flat Detector Computed Tomography Angiography with Intravenous Contrast Application: Feasibility for Visualization of Cerebral Arterial Vasculature. Journal of Neuroimaging. 2013;23(3):414-20.

69. Hoelter P, Goelitz P, Lang S, Luecking H, Kalmuenzer B, Struffert T, et al. Visualization of large vessel occlusion, clot extent, and collateral supply using volume perfusion flat detector computed tomography in acute stroke patients. Acta Radiologica. 2019;60(11):1504-11.

70. Requena M, Olivé-Gadea M, Muchada M, Hernández D, Rubiera M, Boned S, et al. Direct to Angiography Suite Without Stopping for Computed Tomography Imaging for Patients With Acute Stroke: A Randomized Clinical Trial. JAMA Neurology. 2021;78(9):1099-107.

71. Mendez B, Requena M, Aires A, Martins N, Boned S, Rubiera M, et al. Direct Transfer to Angio-Suite to Reduce Workflow Times and Increase Favorable Clinical Outcome. Stroke. 2018;49(11):2723-7.

72. NCT04701684. WE-TRUST (Workflow Optimization to Reduce Time to Endovascular Reperfusion for Ultra-fast Stroke Treatment): clinicaltrials.gov; 2021 [NCT04701684]. Available from: https://clinicaltrials.gov/ct2/show/NCT04701684?id=NCT04701684&draw=2&rank=1&load=cart.

73. Jacobson B. Dichromatic absorption radiography; dichromography. Acta radiol. 1953;39(6):437-52.

74. Fredenberg E. Spectral and dual-energy X-ray imaging for medical applications. Nuclear Instruments and Methods in Physics Research Section A: Accelerators, Spectrometers, Detectors and Associated Equipment. 2018;878:74-87.

75. Alvarez RE, Macovski A. Energy-selective reconstructions in X-ray computerized tomography. Phys Med Biol. 1976;21(5):733-44.

76. Kalender WA, Perman WH, Vetter JR, Klotz E. Evaluation of a prototype dual-energy computed tomographic apparatus. I. Phantom studies. Medical Physics. 1986;13(3):334-9.

77. McCollough CH, Leng S, Yu L, Fletcher JG. Dual- and Multi-Energy CT: Principles, Technical Approaches, and Clinical Applications. Radiology. 2015;276(3):637-53.

78. Mangesius S, Grams AE. Dual energy computed tomomgraphy in acute stroke, where are we and where are we going? Journal of Neuroradiology. 2021;48(2):71-4.

79. Zhou W, Lane JI, Carlson ML, Bruesewitz MR, Witte RJ, Koeller KK, et al. Comparison of a Photon-Counting-Detector CT with an Energy-Integrating-Detector CT for Temporal Bone Imaging: A Cadaveric Study. AJNR American journal of neuroradiology. 2018;39(9):1733-8.

80. Flohr TG, McCollough CH, Bruder H, Petersilka M, Gruber K, Suss C, et al. First performance evaluation of a dual-source CT (DSCT) system. European radiology. 2006;16(2):256-68.

81. Altman A, Carmi R. TU-E-210A-03: A Double-Layer Detector, Dual-Energy CT — Principles, Advantages and Applications. Medical Physics. 2009;36(6Part24):2750-.

82. Zhang D, Li X, Liu B. Objective characterization of GE Discovery CT750 HD scanner: Gemstone spectral imaging mode. Medical Physics. 2011;38(3):1178-88.

83. Euler A, Parakh A, Falkowski AL, Manneck S, Dashti D, Krauss B, et al. Initial Results of a Single-Source Dual-Energy Computed Tomography Technique Using a Split-Filter: Assessment of Image Quality, Radiation Dose, and Accuracy of Dual-Energy Applications in an In Vitro and In Vivo Study. Investigative radiology. 2016;51(8):491-8.

84. Nadav Shapira YY, Naor Wainer, Ami Altman. Spectral Imaging Technologies and Apps and Dual-Layer Detector. In: K. Taguchi IB, K. Iniewski, editor. Spectral, Photon Counting Computed Tomography: Technology and Applications: CRC Press; 2020.

85. Schneider U, Pedroni E, Lomax A. The calibration of CT Hounsfield units for radiotherapy treatment planning. Phys Med Biol. 1996;41(1):111-24.

86. Yang M, Virshup G, Clayton J, Zhu XR, Mohan R, Dong L. Theoretical variance analysis of single- and dual-energy computed tomography methods for calculating proton stopping power ratios of biological tissues. Physics in Medicine and Biology. 2010;55(5):1343-62.

87. Hua C-h, Shapira N, Merchant TE, Klahr P, Yagil Y. Accuracy of electron density, effective atomic number, and iodine concentration determination with a dual-layer dual-energy computed tomography system. Medical Physics. 2018;45(6):2486-97.

88. Nakajima S, Ito H, Mitsuhashi T, Kubo Y, Matsui K, Tanaka I, et al. Clinical application of effective atomic number for classifying non-calcified coronary plaques by dual-energy computed tomography. Atherosclerosis. 2017;261:138-43.

89. Zhu J, Penfold SN. Dosimetric comparison of stopping power calibration with dual-energy CT and single-energy CT in proton therapy treatment planning. Medical Physics. 2016;43(6Part1):2845-54.

90. Pomerantz SR, Kamalian S, Zhang D, Gupta R, Rapalino O, Sahani DV, et al. Virtual monochromatic reconstruction of dual-energy unenhanced head CT at 65-75 keV maximizes image quality compared with conventional polychromatic CT. Radiology. 2013;266(1):318-25.

91. Neuhaus V, Abdullayev N, Grosse Hokamp N, Pahn G, Kabbasch C, Mpotsaris A, et al. Improvement of Image Quality in Unenhanced Dual-Layer CT of the Head Using Virtual Monoenergetic Images Compared With Polyenergetic Single-Energy CT. Invest Radiol. 2017;52(8):470-6.

92. van Ommen F, Kauw F, Bennink E, Heit JJ, Wolman DN, Dankbaar JW, et al. Image Quality of Virtual Monochromatic Reconstructions of Noncontrast CT on a Dual-Source CT Scanner in Adult Patients. Academic Radiology. 2020.

93. Riederer I, Fingerle AA, Baum T, Kirschke JS, Rummeny EJ, Noël PB, et al. Acute infarction after mechanical thrombectomy is better delineable in virtual non-contrast compared to conventional images using a dual-layer spectral CT. Scientific reports. 2018;8(1):9329-.

94. Gariani J, Cuvinciuc V, Courvoisier D, Krauss B, Mendes Pereira V, Sztajzel R, et al. Diagnosis of acute ischemia using dual energy CT after mechanical thrombectomy. Journal of NeuroInterventional Surgery. 2016;8(10):996-1000.

95. Almqvist H, Holmin S, Mazya MV. Dual energy CT after stroke thrombectomy alters assessment of hemorrhagic complications. Neurology. 2019;93(11):e1068-e75.

96. Almqvist H, Almqvist NS, Holmin S, Mazya MV. Dual-Energy CT Follow-Up After Stroke Thrombolysis Alters Assessment of Hemorrhagic Complications. Frontiers in Neurology. 2020;11(357).

97. Schneider D, Apfaltrer P, Sudarski S, Nance JW, Haubenreisser H, Fink C, et al. Optimization of Kiloelectron Volt Settings in Cerebral and Cervical Dual-energy CT Angiography Determined with Virtual Monoenergetic Imaging. Academic Radiology. 2014;21(4):431-6.

98. Leithner D, Mahmoudi S, Wichmann JL, Martin SS, Lenga L, Albrecht MH, et al. Evaluation of virtual monoenergetic imaging algorithms for dual-energy carotid and intracerebral CT angiography: Effects on image quality, artefacts and diagnostic performance for the detection of stenosis. European journal of radiology. 2018;99:111-7.

99. Neuhaus V, Grosse Hokamp N, Abdullayev N, Maus V, Kabbasch C, Mpotsaris A, et al. Comparison of virtual monoenergetic and polyenergetic images reconstructed from dual-layer detector CT angiography of the head and neck. European radiology. 2018;28(3):1102-10.

100. Grams AE, Djurdjevic T, Rehwald R, Schiestl T, Dazinger F, Steiger R, et al. Improved visualisation of early cerebral infarctions after endovascular stroke therapy using dual-energy computed tomography oedema maps. European radiology. 2018;28(11):4534-41.

101. Noguchi K, Itoh T, Naruto N, Takashima S, Tanaka K, Kuroda S. A Novel Imaging Technique (X-Map) to Identify Acute Ischemic Lesions Using Noncontrast Dual-Energy Computed Tomography. J Stroke Cerebrovasc Dis. 2017;26(1):34-41.

102. Taguchi K, Itoh T, Fuld MK, Fournie E, Lee O, Noguchi K. "X-Map 2.0" for Edema Signal Enhancement for Acute Ischemic Stroke Using Non-Contrast-Enhanced Dual-Energy Computed Tomography. Investigative radiology. 2018;53(7):432-9.

103. Mohammed MF, Marais O, Min A, Ferguson D, Jalal S, Khosa F, et al. Unenhanced Dual-Energy Computed Tomography: Visualization of Brain Edema. Invest Radiol. 2018;53(2):63-9.

104. Hixson HR, Leiva-Salinas C, Sumer S, Patrie J, Xin W, Wintermark M. Utilizing dual energy CT to improve CT diagnosis of posterior fossa ischemia. J Neuroradiol. 2016;43(5):346-52.

105. van Ommen F, Dankbaar JW, Zhu G, Wolman DN, Heit JJ, Kauw F, et al. Virtual monochromatic dual-energy CT reconstructions improve detection of cerebral infarct in patients with suspicion of stroke. Neuroradiology. 2020.

106. Borges AP, Antunes C, Curvo-Semedo L. Pros and Cons of Dual-Energy CT Systems: “One Does Not Fit All&rdquo. Tomography. 2023;9(1):195-216.

107. Agostini A, Borgheresi A, Mari A, Floridi C, Bruno F, Carotti M, et al. Dual-energy CT: theoretical principles and clinical applications. Radiol Med. 2019;124(12):1281-95.

108. Mellander H, Fransson V, Ydström K, Lätt J, Ullberg T, Wassélius J, et al. Metal artifact reduction by virtual monoenergetic reconstructions from spectral brain CT. European Journal of Radiology Open. 2023;10.

109. Brown KM, Zabic S, Shechter G. Impact of spectral separation in dual-energy CT with anti-correlated statistical reconstruction. Proceedings of the 13th fully three-dimensional image reconstruction in radiology and nuclear medicine. 2015:491-4.

110. Lennartz S, Laukamp KR, Neuhaus V, Grosse Hokamp N, Le Blanc M, Maus V, et al. Dual-layer detector CT of the head: Initial experience in visualization of intracranial hemorrhage and hypodense brain lesions using virtual monoenergetic images. Eur J Radiol. 2018;108:177-83.

111. Kalisz K, Rassouli N, Dhanantwari A, Jordan D, Rajiah P. Noise characteristics of virtual monoenergetic images from a novel detector-based spectral CT scanner. European journal of radiology. 2018;98:118-25.

112. Zhao X-M, Wang M, Wu R-Z, Dharaiya E, Feng F, Li M-L, et al. Dual-layer spectral detector CT monoenergetic reconstruction improves image quality of non-contrast cerebral CT as compared with conventional single energy CT. European journal of radiology. 2018;103:131-8.

113. Reimer RP, Flatten D, Lichtenstein T, Zopfs D, Neuhaus V, Kabbasch C, et al. Virtual Monoenergetic Images from Spectral Detector CT Enable Radiation Dose Reduction in Unenhanced Cranial CT. AJNR American journal of neuroradiology. 2019;40(10):1617-23.

114. Li H, Giles W, Ren L, Bowsher J, Yin F-F. Implementation of dual-energy technique for virtual monochromatic and linearly mixed CBCTs. Medical physics (Lancaster). 2012;39(10):6056-64.

115. Zbijewski W, Gang GJ, Xu J, Wang AS, Stayman JW, Taguchi K, et al. Dual-energy cone-beam CT with a flat-panel detector: effect of reconstruction algorithm on material classification. Med Phys. 2014;41(2):021908.

116. Men K, Dai J, Chen X, Li M, Zhang K, Huang P. Dual-energy imaging method to improve the image quality and the accuracy of dose calculation for cone-beam computed tomography. Physica Medica: European Journal of Medical Physics. 2017;36:110-8.

117. Skaarup M, Edmund JM, Dorn S, Kachelriess M, Vogelius IR. Dual-energy material decomposition for cone-beam computed tomography in image-guided radiotherapy. Acta Oncol. 2019;58(10):1483-8.

118. Sajja S, Lee Y, Eriksson M, Nordström H, Sahgal A, Hashemi M, et al. Technical Principles of Dual-Energy Cone Beam Computed Tomography and Clinical Applications for Radiation Therapy. Adv Radiat Oncol. 2020;5(1):1-16.

119. Müller K, Datta S, Ahmad M, Choi J-H, Moore T, Pung L, et al. Interventional dual-energy imaging—Feasibility of rapid kV-switching on a C-arm CT system. Medical Physics. 2016;43(10):5537-46.

120. Myronakis M, Fueglistaller R, Rottmann J, Hu YH, Wang A, Baturin P, et al. Spectral imaging using clinical megavoltage beams and a novel multi-layer imager. Phys Med Biol. 2017;62(23):9127-39.

121. Shi L, Lu M, Bennett NR, Shapiro E, Zhang J, Colbeth R, et al. Characterization and potential applications of a dual-layer flat-panel detector. Medical Physics. 2020;47(8):3332-43.

122. Demeestere J, Scheldeman L, Cornelissen SA, Heye S, Wouters A, Dupont P, et al. Alberta Stroke Program Early CT Score Versus Computed Tomographic Perfusion to Predict Functional Outcome After Successful Reperfusion in Acute Ischemic Stroke. Stroke. 2018;49(10):2361-7.

123. Haranhalli N, Mbabuike N, Grewal SS, Hasan TF, Heckman MG, Freeman WD, et al. Topographic correlation of infarct area on CT perfusion with functional outcome in acute ischemic stroke. J Neurosurg. 2019:1-9.

124. Schregel K, Tsogkas I, Peter C, Zapf A, Behme D, Schnieder M, et al. Outcome Prediction Using Perfusion Parameters and Collateral Scores of Multi-Phase and Single-Phase CT Angiography in Acute Stroke: Need for One, Two, Three, or Thirty Scans? J Stroke. 2018;20(3):362-72.

125. Janssen PM, Venema E, Dippel DWJ. Effect of Workflow Improvements in Endovascular Stroke Treatment. Stroke. 2019;50(3):665-74.

126. Brehm A, Tsogkas I, Maier IL, Eisenberger HJ, Yang P, Liu JM, et al. One-Stop Management with Perfusion for Transfer Patients with Stroke due to a Large-Vessel Occlusion: Feasibility and Effects on In-Hospital Times. AJNR American journal of neuroradiology. 2019;40(8):1330-4.

127. Saver JL. Time is brain--quantified. Stroke. 2006;37(1):263-6.

128. Saver JL, Goyal M, van der Lugt A, Menon BK, Majoie CB, Dippel DW, et al. Time to Treatment With Endovascular Thrombectomy and Outcomes From Ischemic Stroke: A Meta-analysis. Jama. 2016;316(12):1279-88.

129. Genders TS, Spronk S, Stijnen T, Steyerberg EW, Lesaffre E, Hunink MG. Methods for calculating sensitivity and specificity of clustered data: a tutorial. Radiology. 2012;265(3):910-6.

130. Brown LD, Cai TT, DasGupta A. Interval Estimation for a Binomial Proportion. Statistical Science. 2001;16(2):101-17.

131. Mercaldo ND, Lau KF, Zhou XH. Confidence intervals for predictive values with an emphasis to case–control studies. Statistics in Medicine. 2007;26(10):2170-83.

132. Bujila R, Omar A, Poludniowski G. A validation of SpekPy: A software toolkit for modelling X-ray tube spectra. Phys Med. 2020;75:44-54.

133. XCOM: Photon Cross Section Database (version 1.5). [Internet]. National Institute of Standards and Technology. 2010 [cited 2021, April 2]. Available from: http://physics.nist.gov/xcom.

134. Keselman B, Berglund A, Ahmed N, Bottai M, Euler Mv, Holmin S, et al. The Stockholm Stroke Triage Project: Outcomes of Endovascular Thrombectomy Before and After Triage Implementation. Stroke. 2022;53(2):473-81.

135. Hinkmann FM, Voit HL, Anders K, Baum U, Seidensticker P, Bautz WA, et al. Ultra-Fast Carotid CT-Angiography: Low Versus Standard Volume Contrast Material Protocol for a 128-Slice CT-System. Investigative radiology. 2009;44(5).

136. Mantel N, Haenszel W. Statistical aspects of the analysis of data from retrospective studies of disease. J Natl Cancer Inst. 1959;22(4):719-48.

137. Conger AJ. Integration and generalization of kappas for multiple raters. Psychol Bull. 1980;88:322-8.

138. Nicholson P, Hilditch CA, Neuhaus A, Seyedsaadat SM, Benson JC, Mark I, et al. Per-region interobserver agreement of Alberta Stroke Program Early CT Scores (ASPECTS). Journal of neurointerventional surgery. 2020.

139. Fleiss JL. Measuring nominal scale agreement among many raters. Psychol Bull. 1971;76(5):378-82.

140. Viera AJ, Garrett JM. Understanding interobserver agreement: the kappa statistic. Fam Med. 2005;37(5):360-3.

141. The 2007 Recommendations of the International Commission on Radiological Protection. ICRP publication 103. Ann ICRP. 2007;37(2-4):1-332.

142. 1990 Recommendations of the International Commission on Radiological Protection. Ann ICRP. 1991;21(1-3):1-201.

143. Folkhälsomyndigheten. Folkhälsan i Sverige 2016 2016 [Available from: https://www.folkhalsomyndigheten.se/publicerat-material/publikationsarkiv/f/folkhalsan-i-sverige-2016/.

144. SURF. Nationella Rekommendationer för Jodkontrastmedel: Svensk Förening för Medicinsk Radiologi; 2017 [Available from: http://www.sfbfm.se/sidor/kontrastmedelsrekommendationer/.

145. Dodig D, Matana Kaštelan Z, Bartolović N, Jurković S, Miletić D, Rumboldt Z. Virtual monoenergetic dual-energy CT reconstructions at 80 keV are optimal non-contrast CT technique for early stroke detection. Neuroradiol J. 2021:19714009211047449.

146. Mellander H, Bengtsson P, Fransson V, Ramgren B, Undrén P, Drake M, et al. Virtual monoenergetic images by spectral detector computed tomography may improve image quality and diagnostic ability for ischemic lesions in acute ischemic stroke. Acta Radiologica. 2023;64(4):1631-40.

147. Matsumoto K, Jinzaki M, Tanami Y, Ueno A, Yamada M, Kuribayashi S. Virtual Monochromatic Spectral Imaging with Fast Kilovoltage Switching: Improved Image Quality as Compared with That Obtained with Conventional 120-kVp CT. Radiology. 2011;259(1):257-62.

148. Yu L, Christner JA, Leng S, Wang J, Fletcher JG, McCollough CH. Virtual monochromatic imaging in dual-source dual-energy CT: radiation dose and image quality. Med Phys. 2011;38(12):6371-9.

149. DiNitto J, Ramirez-Giraldo JC, Froehler M. A novel approach to calculating dual energy in the angiography suite: SPIE; 2021.

150. Grant KL, Flohr TG, Krauss B, Sedlmair M, Thomas C, Schmidt B. Assessment of an Advanced Image-Based Technique to Calculate Virtual Monoenergetic Computed Tomographic Images From a Dual-Energy Examination to Improve Contrast-To-Noise Ratio in Examinations Using Iodinated Contrast Media. Investigative radiology. 2014;49(9):586-92.

151. Petroulia VD, Kaesmacher J, Piechowiak EI, Dobrocky T, Pilgram-Pastor SM, Gralla J, et al. Evaluation of Sine Spin flat detector CT imaging compared with multidetector CT. Journal of neurointerventional surgery. 2022.

152. Zidan M, Ghaei S, Bode FJ, Weller JM, Krueger N, Lehnen NC, et al. Clinical significance and prevalence of subarachnoid hyperdensities on flat detector CT after mechanical thrombectomy: does it really matter? Journal of neurointerventional surgery. 2023.

153. Kauw F, Ding VY, Dankbaar JW, Ommen Fv, Zhu G, Boothroyd DB, et al. Detection of Early Ischemic Changes with Virtual Noncontrast Dual-Energy CT in Acute Ischemic Stroke: A Noninferiority Analysis. American Journal of Neuroradiology. 2022.

154. DiNitto J, Feldman M, Grimaudo H, Mummareddy N, Ahn S, Bhamidipati A, et al. Flat-panel dual-energy head computed tomography in the angiography suite after thrombectomy for acute stroke: A clinical feasibility study. Interv Neuroradiol. 2023:15910199231157462.

155. Cancelliere NM, Hummel E, van Nijnatten F, van de Haar P, Withagen P, van Vlimmeren M, et al. The butterfly effect: improving brain cone-beam CT image artifacts for stroke assessment using a novel dual-axis trajectory. Journal of neurointerventional surgery. 2022:neurintsurg-2021-018553.

156. van Hamersvelt RW, Eijsvoogel NG, Mihl C, de Jong PA, Schilham AMR, Buls N, et al. Contrast agent concentration optimization in CTA using low tube voltage and dual-energy CT in multiple vendors: a phantom study. The International Journal of Cardiovascular Imaging. 2018;34(8):1265-75.

157. Zopfs D, Lennartz S, Abdullayev N, Lichtenstein T, Laukamp KR, Reimer RP, et al. Generally applicable window settings of low-keV virtual monoenergetic reconstructions in dual-layer CT-angiography of the head and neck. Quant Imaging Med Surg. 2021;11(8):3408-17.

158. Ouadah S, Jacobson M, Stayman JW, Ehtiati T, Weiss C, Siewerdsen JH. Correction of patient motion in cone-beam CT using 3D–2D registration. Physics in Medicine & Biology. 2017;62(23):8813-31.

159. Li Y, Garrett JW, Li K, Wu Y, Johnson K, Schafer S, et al. Time-resolved C-arm cone beam CT angiography (TR-CBCTA) imaging from a single short-scan C-arm cone beam CT acquisition with intra-arterial contrast injection. Physics in Medicine & Biology. 2018;63(7):075001.

160. Cancelliere NM, Nijnatten Fv, Hummel E, Withagen P, Haar Pvd, Nishi H, et al. Motion artifact correction for cone beam CT stroke imaging: a prospective series. Journal of neurointerventional surgery. 2022:neurintsurg-2021-018201.

161. Wardlaw JM, Mair G, Kummer Rv, Williams MC, Li W, Storkey AJ, et al. Accuracy of Automated Computer-Aided Diagnosis for Stroke Imaging: A Critical Evaluation of Current Evidence. Stroke. 2022;53(7):2393-403.

162. Snapinn SM. Noninferiority trials. Curr Control Trials Cardiovasc Med. 2000;1(1):19-21.

163. CLOPPER CJ, PEARSON ES. THE USE OF CONFIDENCE OR FIDUCIAL LIMITS ILLUSTRATED IN THE CASE OF THE BINOMIAL. Biometrika. 1934;26(4):404-13.

164. Raz E, Nossek E, Sahlein DH, Sharashidze V, Narayan V, Ali A, et al. Principles, techniques and applications of high resolution cone beam CT angiography in the neuroangio suite. Journal of neurointerventional surgery. 2023;15(6):600-7.

165. Forghani R, De Man B, Gupta R. Dual-Energy Computed Tomography. Neuroimaging Clinics of North America. 2017;27(3):371-84.

166. Šimundić AM. Measures of Diagnostic Accuracy: Basic Definitions. Ejifcc. 2009;19(4):203-11.

167. Alberg AJ, Park JW, Hager BW, Brock MV, Diener-West M. The use of "overall accuracy" to evaluate the validity of screening or diagnostic tests. J Gen Intern Med. 2004;19(5 Pt 1):460-5.

168. Yoshimura S, Sakai N, Yamagami H, Uchida K, Beppu M, Toyoda K, et al. Endovascular Therapy for Acute Stroke with a Large Ischemic Region. New England Journal of Medicine. 2022;386(14):1303-13.

169. Huo X, Ma G, Tong X, Zhang X, Pan Y, Nguyen TN, et al. Trial of Endovascular Therapy for Acute Ischemic Stroke with Large Infarct. New England Journal of Medicine. 2023;388(14):1272-83.

170. Sarraj A, Hassan AE, Abraham MG, Ortega-Gutierrez S, Kasner SE, Hussain MS, et al. Trial of Endovascular Thrombectomy for Large Ischemic Strokes. New England Journal of Medicine. 2023;388(14):1259-71.

171. University Hospital B, Switzerland. ProSPective Evaluation of Non-contrast sINe spiN Flat-dEtectoR CT for the Detection of Intracranial hemorrhageS (SPINNERS): Clinicaltrials.gov; 2023 [Available from: https://classic.clinicaltrials.gov/ct2/show/NCT05458908.

172. Willemink MJ, Persson M, Pourmorteza A, Pelc NJ, Fleischmann D. Photon-counting CT: Technical Principles and Clinical Prospects. Radiology. 2018;289(2):293-312.

173. Si-Mohamed SA, Boccalini S, Villien M, Yagil Y, Erhard K, Boussel L, et al. First Experience With a Whole-Body Spectral Photon-Counting CT Clinical Prototype. Investigative radiology. 2023;58(7):459-71.

174. van der Bie J, van Straten M, Booij R, Bos D, Dijkshoorn ML, Hirsch A, et al. Photon-counting CT: Review of initial clinical results. European journal of radiology. 2023;163:110829.

175. Hsieh SS, Leng S, Rajendran K, Tao S, McCollough CH. Photon Counting CT: Clinical Applications and Future Developments. IEEE Trans Radiat Plasma Med Sci. 2021;5(4):441-52.

176. Danielsson M, Persson M, Sjölin M. Photon-counting x-ray detectors for CT. Physics in Medicine & Biology. 2021;66(3):03TR1.

177. Pourmorteza A, Symons R, Reich DS, Bagheri M, Cork TE, Kappler S, et al. Photon-Counting CT of the Brain: In Vivo Human Results and Image-Quality Assessment. AJNR American journal of neuroradiology. 2017;38(12):2257-63.

178. Treb K, Ji X, Feng M, Zhang R, Periyasamy S, Laeseke PF, et al. A C-arm photon counting CT prototype with volumetric coverage using multi-sweep step-and-shoot acquisitions. Physics in Medicine & Biology. 2022;67(21):215003.

179. Treb K, Hämisch Y, Ullberg C, Zhang R, Li K. Photon counting-energy integrating hybrid flat panel detector systems for image-guided interventions: an experimental proof-of-concept. Physics in Medicine & Biology. 2023;68(13):135009.